

High-Risk Long QT Syndrome Mutations in the Kv7.1 (KCNQ1) Pore Disrupt the Molecular Basis for Rapid K⁺ Permeation

Don E. Burgess,[†] Daniel C. Bartos,[†] Allison R. Relej,[†] Kenneth S. Campbell,[†] Jonathan N. Johnson,[‡] David J. Tester,[‡] Michael J. Ackerman,[‡] Véronique Fressart,^{§,||} Isabelle Denjoy,^{§,||} Pascale Guicheney,^{§,||} Arthur J. Moss,[⊥] Seiko Ohno,[@] Minoru Horie,[@] and Brian P. Delisle^{*,†}

[†]Center for Muscle Biology, Department of Physiology, University of Kentucky, 800 Rose Street, MS508, Lexington, Kentucky 40536, United States

[‡]Departments of Medicine, Pediatrics, and Molecular Pharmacology and Experimental Therapeutics/Divisions of Cardiovascular Diseases and Pediatric Cardiology, Mayo Clinic, Rochester, Minnesota 55905, United States

[§]INSERM, U956, Hôpital Pitié-Salpêtrière, Fondation ICAN, Paris, France

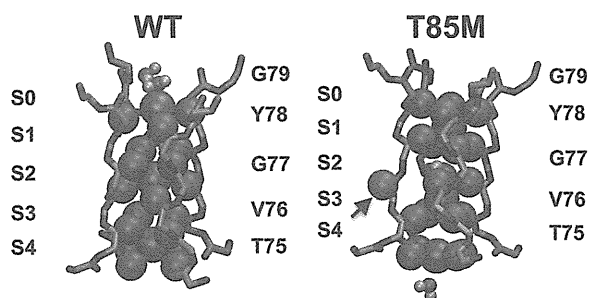
^{||}UPMC Univ Paris 06, UMR_S956, IFR14, Paris, France

[⊥]Department of Medicine, University of Rochester Medical Center, Rochester, New York 14642, United States

[@]Department of Cardiovascular and Respiratory Medicine, Shiga University of Medical Sciences, Seta-tsukinowa, Ohtsu 520-2192, Japan

Supporting Information

ABSTRACT: Type 1 long QT syndrome (LQT1) is caused by loss-of-function mutations in the *KCNQ1* gene, which encodes the K⁺ channel (Kv7.1) that underlies the slowly activating delayed rectifier K⁺ current in the heart. Intragenic risk stratification suggests LQT1 mutations that disrupt conserved amino acid residues in the pore are an independent risk factor for LQT1-related cardiac events. The purpose of this study is to determine possible molecular mechanisms that underlie the loss of function for these high-risk mutations. Extensive genotype–phenotype analyses of LQT1 patients showed that T322M-, T322A-, or G325R-Kv7.1 confers a high risk for LQT1-related cardiac events. Heterologous expression of these mutations with KCNE1 revealed they generated nonfunctional channels and caused dominant negative suppression of WT-Kv7.1 current. Molecular dynamics simulations of analogous mutations in KcsA (T85M-, T85A-, and G88R-KcsA) demonstrated that they disrupted the symmetrical distribution of the carbonyl oxygen atoms in the selectivity filter, which upset the balance between the strong attractive and K⁺–K⁺ repulsive forces required for rapid K⁺ permeation. We conclude high-risk LQT1 mutations in the pore likely disrupt the architectural and physical properties of the K⁺ channel selectivity filter.



Congenital long QT syndrome (LQTS) is a monogenic cardiac arrhythmia syndrome that occurs in ~1 in 2500 people and increases the risk for polymorphic ventricular tachycardia (torsades de pointes or torsades), syncope, and sudden death.^{1–3} Type 1 long QT syndrome (LQT1) accounts for ~35% of LQTS and is caused by loss-of-function mutations in the *KCNQ1* K⁺ channel (Kv7.1).^{4–12} Kv7.1 combines with the β -subunit KCNE1 to mediate the slowly activating delayed rectifier K⁺ current in the heart (I_{Ks}). Intragenic risk stratification shows patients who have LQT1 missense mutations at conserved amino acids in the pore correlate with an increased risk for cardiac events (independent of QTc interval, gender, or β -blocker therapy).¹³ The purpose of this study was to identify possible molecular mechanisms that underlie the loss of function for these high-risk LQT1 mutations.

The pore domain for all K⁺ channels is composed of two transmembrane segments joined together by a linker that contains the conserved amino acids of the selectivity filter. X-ray analysis of a K⁺ channel pore from *Streptomyces lividans* (KcsA) showed that the selectivity filter forms four contiguous K⁺ binding sites (S1–S4).¹⁴ On the basis of this structure, and molecular dynamics simulations (MDS) that calculate the energetics of permeation, the conduction of K⁺ through the selectivity filter occurs by transitioning between two global states where two K⁺ ions occupy S4 and S2, or S3 and S1.^{15–21} The energetics for K⁺ ions moving between these binding sites is essentially barrierless, but short-range K⁺–K⁺ repulsion

Received: July 16, 2012

Revised: October 23, 2012

Published: October 23, 2012

between the ions is essential for promoting the exit of the K⁺ ion from S1 to a weak binding site outside the pore (S0).^{15,19}

The KcsA selectivity filter is nearly identical to Kv7.1 (as well as most other K⁺ selective channels). We made the simplifying assumption that the conserved amino acids in KcsA and Kv7.1 selectivity filters are structurally and functionally similar. This allowed us to study the impact of high-risk LQT1 pore mutations using the KcsA crystal structure. The advantage to using the KcsA structure is that it has been widely used to model K⁺ ion permeation,^{15–17,19,21,22} and similar to KCNE1-modified Kv7.1 channels, MDS show that the KcsA selectivity filter does not readily transit to nonconducting or inactivated states.^{15,22}

EXPERIMENTAL PROCEDURES

Clinical. We identified more than 60 patients heterozygous for LQT1 missense mutations that disrupt a highly conserved threonine or glycine near the selectivity filter (T322M-, T322A-, or G325R-Kv7.1) (Table 1 and Table 1 of the

Table 1. Clinical Characteristics for Genotype Positive Patients with T322M-, T322A-, or G325R-Kv7.1^a

no. of genotype positive families	26
no. with family history of symptoms	22
no. with T322M	13
no. with family history of symptoms	9
no. with T322A	2
no. with family history of symptoms	2
no. with G325R	11
no. with family history of symptoms	11
no. of genotype positive subjects (female, male)	63 (35, 28)
no. of symptomatic	29 (19, 10)
mean QTc ± SD (ms)	483 ± 44 (490 ± 32, 473 ± 55)
average age ± SD (years)	29 ± 18 (31 ± 20, 26 ± 17)
no. with T322M	29 (16, 13)
no. of symptomatic	12 (7, 5)
mean QTc ± SD (ms)	497 ± 43 (505 ± 32, 488 ± 54)
average age ± SD (years)	29 ± 18 (29 ± 20, 26 ± 16)
no. with T322A	12 (7, 5)
no. of symptomatic	2 (2, 0)
mean QTc ± SD (ms)	463 ± 27 (473 ± 22, 447 ± 27)
average age ± SD (years)	20 ± 16 (24 ± 18, 15 ± 12)
no. with G325R	22 (12, 10)
no. of symptomatic	15 (10, 5)
mean QTc ± SD (ms)	474 ± 47 (479 ± 31, 468 ± 63)
average age ± SD (years)	35 ± 19 (39 ± 20, 30 ± 18)

^aSymptomatic is defined as experiencing syncope, torsades, or near drowning. See Table 1 of the Supporting Information for individual patient details.

Supporting Information).^{23,24} One of these families (O) was reported previously.²⁵ Individual patient details are provided in Table 1 of the Supporting Information. The study was conducted according to the principles of the Helsinki Declaration. Blood samples were obtained after signed written informed consent for genetic analyses and after approval by the local institutional ethics committees. The respective protocols

for research-based or commercially available genetic analyses of patients with LQTS were performed. Genomic DNA was isolated from blood leukocytes, and mutational analyses were performed using standard methods. The index patients in the families are negative for additional LQTS-associated mutations in both *KCNQ1* and the major LQTS susceptibility genes (except for the index patient in family A who has yet to be tested).

Mutagenesis, Transfection, Electrophysiology, and Biotinylation. The appropriate nucleotide changes to generate the T322M-, T322A-, and G325R-Kv7.1 mutants were introduced into WT-Kv7.1 cDNA and used for electrophysiological studies in HEK293 cells as previously described.²⁶ To recapitulate *I_{Ks}*-like currents, all transfections included equal amounts of Kv7.1 and the auxiliary Kv7.1 β-subunit KCNE1 plasmid DNA (3 μg each). For coexpression studies, equal amounts of WT-Kv7.1 (1.5 μg) and mutant Kv7.1 (1.5 μg) were used to maintain the equivalent Kv7.1 plasmid DNA concentration (3 μg). The cells were cultured in MEM (with 10% fetal bovine serum) at 37 °C, and functional analyses were conducted using the standard whole-cell patch clamp technique 24–30 h after transfection. The external solution contained 137 mM NaCl, 4 mM KCl, 1.8 mM CaCl₂, 1 mM MgCl₂, 10 mM glucose, and 10 mM HEPES (pH 7.4 with NaOH), and an internal pipet solution contained 130 mM KCl, 1 mM MgCl₂, 5 mM EDTA, 5 mM MgATP, and 10 mM HEPES (pH 7.2 with KOH). An Axopatch-200B patch clamp amplifier (Axon Instruments, Union City, CA) was used to measure membrane currents and cell capacitance. Only cells with stable membrane resistances of >1 GΩ were studied. pCLAMP 10.0 (Axon Instruments) was used to generate the voltage clamp protocols, to acquire current signals, and to analyze data. Origin 7.0 (Microcal, Northhampton, MA) was used to perform Boltzmann fitting, to generate current–voltage (*I*–*V*) relations, and to plot graphs. The Boltzmann equation used to describe the *I*–*V* relations was

$$I = (I_{\text{MIN}} - I_{\text{MAX}}) / [1 + e^{(V - V_{1/2})/k}] + I_{\text{MAX}}$$

where *I*_{MIN} is the minimally activated current, *I*_{MAX} is the maximally activated current, *V*_{1/2} is the midpoint potential for half-maximal activation, and *k* is the slope factor (millivolts per e-fold change). For all experiments, the holding potential was –80 mV, and the dotted line in figures corresponds to the zero-current baseline. Voltage clamp experiments were performed at 22–23 °C within 1–2 h of the removal of cells from their culture conditions.

The biotinylation procedure was described previously.²⁶ Western blots of the biotinylated proteins were analyzed using the Odyssey infrared imaging system (Li-Cor, Lincoln, NE). The membranes were incubated in anti-Kv7.1 (Alomone laboratories, Jerusalem, Israel) and anti-Na⁺/K⁺-ATPase (Abcam, Cambridge, MA) to normalize for the biotinylation reaction. The appropriate IRdye secondary antibodies (Li-Cor) were used to detect anti-Kv7.1 and anti-Na⁺/K⁺-ATPase. To ensure that the cell surface biotinylation did not label intracellular proteins, the samples were probed with anti-calnexin (Abcam). Odyssey (Li-Cor) was used to quantify the density of the protein bands. The relative intensity of Kv7.1 to Na⁺/K⁺-ATPase intensity was calculated by normalizing the intensity of the Kv7.1 signal to the intensity of the Na⁺/K⁺-ATPase signal.

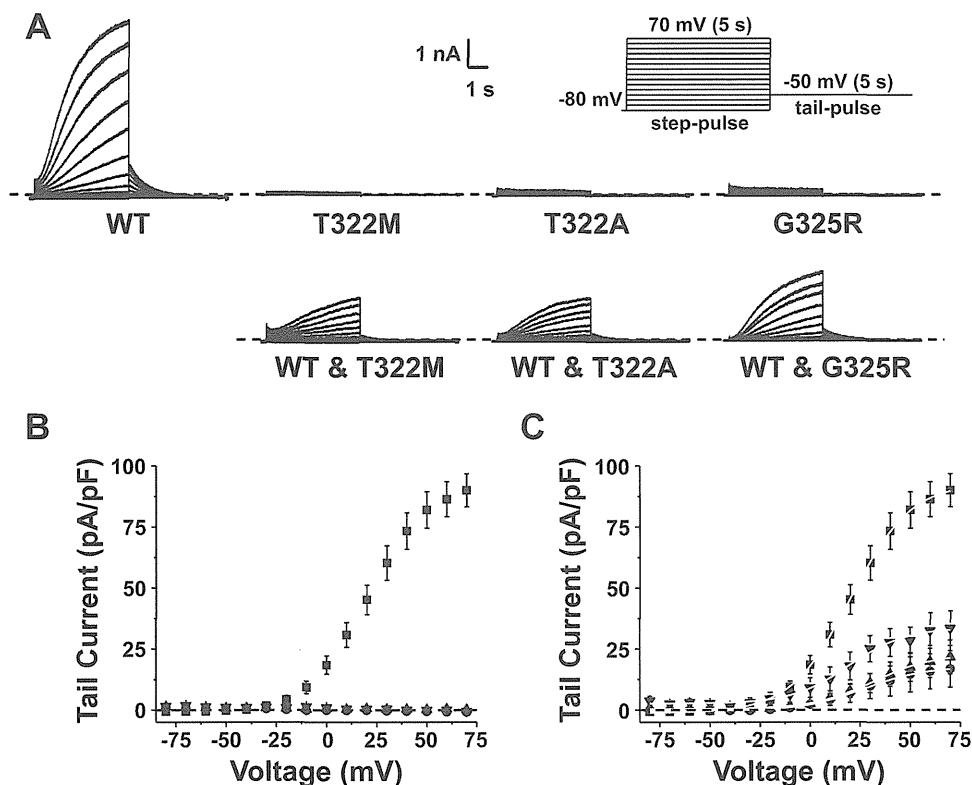


Figure 1. T322M-, T322A-, and G325R-Kv7.1 generate nonfunctional channels and cause dominant negative suppression of WT-Kv7.1 current. (A) Representative families of currents recorded from cells expressing WT-, T322M-, T322A-, or G325R-Kv7.1 using the voltage protocol shown. Also shown are representative families of currents from cells coexpressing WT- and T322M-, T322A-, or G325R-Kv7.1. (B) The graph shows the corresponding mean $I-V$ relations for the peak tail current plotted as a function of the test voltage for WT-Kv7.1 (black filled squares), T322M-Kv7.1 (gray filled circles), T322A-Kv7.1 (gray upward-pointing triangles), or G325R-Kv7.1 (gray downward-pointing triangles). (C) The graph shows the corresponding mean $I-V$ relations for the peak tail current plotted as a function of the test voltage for WT-Kv7.1 (black filled squares), WT- and T322M-Kv7.1 (gray filled circles), WT- and T322A-Kv7.1 (gray upward-pointing triangles), or WT- and G325R-Kv7.1 (gray downward-pointing triangles). The mean peak $I-V$ relations were described using a Boltzmann equation (gray line). All of these studies included KCNE1.

Molecular Dynamics Simulations. Details regarding the MDS are provided in the Supporting Information. Briefly, the MDS systems for the KcsA channels (Protein Data Bank entry 1k4c)²⁷ were constructed using Visual Molecular Dynamics (VMD),²⁸ and KcsA simulations were performed using NAMD (Not just Another Molecular Dynamics program).²⁹ The KcsA structure was used to generate a channel embedded in a lipid bilayer consisting of 1-palmitoyl-2-palmitoleoyl-*sn*-glycero-3-phosphocholine (POPC) molecules, with explicit water, K^+ ions, and Cl^- ions. Two K^+ ions were placed in the selectivity filter, and one was placed in the cavity. A series of short MDS were performed to equilibrate the system as a whole. Production simulations were performed for up to 60 ns. A time step of 2 fs was employed in all simulations, and the atomic trajectory data were written at 1 ps intervals. VMD was used to analyze the atomic trajectories. MDS showed that the root-mean-square deviation (rmsd) values for α -carbon (C_α) backbone and amino acids quickly reached steady state after 5 ns. The relative rmsd values for the WT and mutant simulations were similar to one another (data not shown), suggesting that the mutations did not grossly affect channel stability.

Statistical Analysis. Data are reported as the mean \pm the standard error (SE) unless otherwise noted. A one-way analysis of variance with a Bonferroni post hoc test was used to determine if either of the mutant parameters differed from that of WT ($p < 0.05$ was considered significant).

RESULTS

The purpose of this study is to identify the possible molecular mechanisms for high-risk LQT1 mutations in the pore domain. Because of the wide range of LQT1 expressivity in patients, a large number of patients with the same mutation need to be studied to confirm that they confer a high risk for LQT1-related cardiac events. We identified more than 60 patients from 26 families that are heterozygous for LQT1 mutations T322M-, T322A-, and G325R-Kv7.1 (Figure 1, Table 1, and Table 1 of the Supporting Information).¹¹ More than one-third of the patients have marked QT prolongation ($QTc \geq 500$ ms), and $\sim 85\%$ of these families have histories of syncope, torsades, near drowning, or sudden cardiac death triggered primarily by exercise or swimming.³⁰ Overall, the clinical data from this large cohort suggested that T322M-, T322A-, and G325R-Kv7.1 confer a high risk for LQT1-related events.

We studied the functional phenotypes for these mutations by voltage-clamping cells transiently expressing WT-, T322M-, T322A-, or G325R-Kv7.1 with KCNE1 (Figure 1A). Macroscopic currents were recorded by applying steplike pulses from -80 to 70 mV in 10 mV increments for 5 s, followed by a "tail" pulse for 5 s to -50 mV (Figure 1A). The peak current amplitude recorded at the start of the tail pulse was plotted as a function of the step pulse potential for cells expressing WT-, T322M-, T322A-, or G325R-Kv7.1 (Figure 1B). To mimic the patients' heterozygous genotype, we also studied cells coexpressing WT- and T322M-, T322A-, or G325R-Kv7.1 (Figure 1A,C). Cells expressing WT-Kv7.1 generated large currents that resembled native I_{Ks} ; cells expressing T322M-, T322A-, or G325R-Kv7.1 did not generate current, and cells coexpressing WT- and T322M-Kv7.1, T322A-Kv7.1, or G325R-Kv7.1 conducted only small currents (Figure 1B). The $I-V$ relations for the peak tail current were plotted as a function of the step voltage, and the data were described with a Boltzmann function to calculate changes in I_{MAX} , $V_{1/2}$, and k . Cells coexpressing WT- and T322M-Kv7.1, T322A-Kv7.1, or G325R-Kv7.1 reduced the I_{MAX} by ~70% with only small changes in activation gating (Table 2 of the Supporting Information). Importantly, the loss-of-function phenotype was not linked to coexpression of KCNE1, because cells expressing WT-, T322M-, T322A-, or G325R-Kv7.1 without KCNE1 showed that the mutations still did not generate any current (data not shown). These data demonstrate that T322M-, T322A-, and G325R-Kv7.1 caused a complete loss of Kv7.1 current and dominant negative suppression of WT-Kv7.1 current.

We tested whether T322M-, T322A-, and G325R-Kv7.1 caused a loss of function by simply reducing the amount of Kv7.1 expressed at the cell surface membrane. Biotinylation assays showed that cells expressing T322M-, T322A-, or G325R-Kv7.1 and KCNE1 reduced the level of cell surface membrane expression of Kv7.1 (Figure 1A,C of the Supporting Information). However, the reduction was insufficient to explain a complete loss of current (Figure 1A,B). Additionally, although cells coexpressing WT-Kv7.1 and T322M-, T322A-, or G325R-Kv7.1 showed dominant negative functional effects (Figure 1A,C), they did not show a decrease in the level of Kv7.1 at the cell surface membrane (Figure 1B,C of the Supporting Information). Together, these data suggest that a decrease in the level of Kv7.1 expression at the cell surface membrane does not account for the mutations' complete loss-of-function or dominant negative phenotypes.

The mutated threonine and glycine are highly conserved pore residues in the K^+ channel family (Figure 2A). Given their proximity to the K^+ channel selectivity filter (Figure 2B), we tested whether incorporating analogous mutations into the KcsA structure altered the architecture of the selectivity filter and permeation events. Panels C-F of Figure 2 show representative MDS images for the WT-, T85M-, T85A-, and G88R-KcsA selectivity filters, respectively. The WT-KcsA selectivity filter formed four contiguous sites that could bind to K^+ ions and water molecules in an alternating manner. For the most part, the oxygen atoms that lined the WT-KcsA selectivity filter faced the central pore axis; however, similar to what has been shown by others,^{17,21,22} the carbonyl oxygen atom between S2 and S3 (V76) on each α -subunit could briefly "flip" away from the central pore axis (Movie 1 of the Supporting Information). The representative selectivity filter images for the T85M-, T85A-, and G88R-KcsA simulations

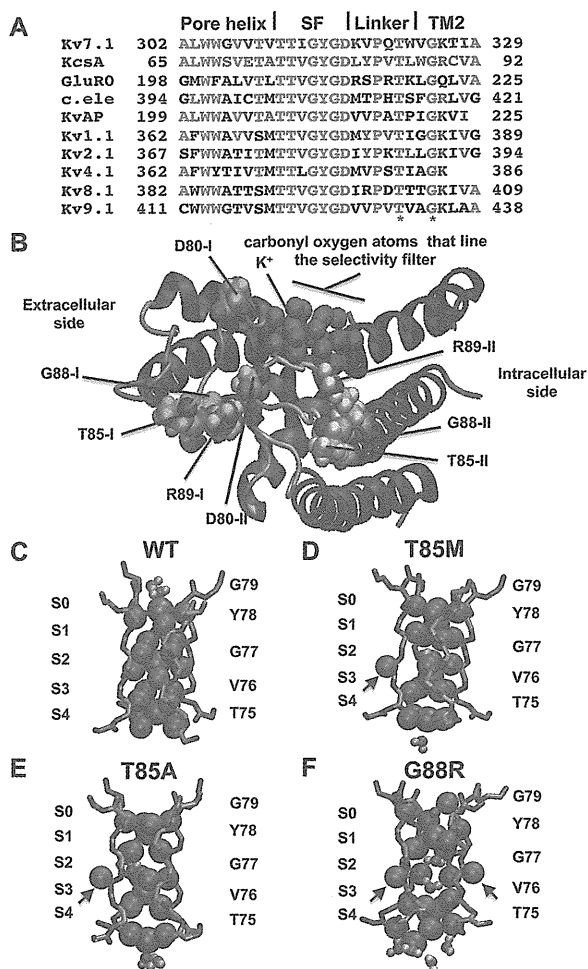


Figure 2. Sequence alignment of the K^+ channel pore domain and the position of the conserved threonine and glycine with respect to the K^+ channel selectivity filter. (A) Sequence alignments of the selectivity filter for different K^+ channels: Kv7.1 (GenBank entry NP_000208NP_000209); KcsA (GenBank entry NP_000208NP_631700.1); GluR0, ionotropic glutamate receptor from *Nostoc punctiforme* (Swiss-Prot entry P73797); c. ele, voltage-dependent K^+ channel from *Caenorhabditis elegans* (GenBank entry AAB95119.1); KvAP, voltage-dependent K^+ channel from *Aeropyrum pernix* (Swiss-Prot entry Q9YDF8.1); Kv1.1 (GenBank entry NP_000208); Kv2.1 (GenBank entry AAB88808.1); Kv4.1 (GenBank entry NP_004970.3); Kv8.1 (GenBank entry NP_055194.1); Kv9.1 (GenBank entry NP_002242.2). Only amino acid residues that correspond to the pore helix, the selectivity filter (SF), and the linker between the selectivity filter and the second transmembrane segment (TM2) in the pore domain are shown. The asterisks denote the conserved threonine and glycine disrupted by T322M-, T322A-, and G325R-Kv7.1 mutations. Red residues are conserved in Kv7.1 and KcsA. Blue residues are conserved in Kv7.1 but not KcsA. Green residues are conserved in KcsA but not Kv7.1. Black residues are not conserved in Kv7.1 or KcsA. (B) Ribbon structure of two adjacent KcsA α -subunits (I and II) (purple) with the space filled van der Waals spheres for the conserved threonine (T85) and glycine (G88) (light blue for C, red for O, dark blue for N, and gray for H); the glycine atoms are all colored yellow for the sake of clarity). Also shown are the van der Waals spheres for the conserved aspartate in the K^+ channel selectivity filter (D80), conserved arginine/lysine (R89), the carbonyl oxygen atoms that line the selectivity filter from all four α -subunits,

Figure 2. continued

and the K^+ ions (green) in the selectivity filter. The threonine and glycine are in the proximity of the aspartate in the selectivity filter of the adjacent subunit. (C–F) Representative atomic-scale image of the selectivity filter for (C) WT-, (D) T85M-, (E) T85A-, or (F) G88R-KcsA MDS. Shown are the main chain backbones for selectivity filter residues TVGYG (light blue for C, red for O, and dark blue for N) for all four α -subunits, the bound K^+ ions (green), and several adjacent water molecules (red for O and gray for H). The oxygen atoms that line the filter and the K^+ ions are shown as large spheres, and water molecules are shown as small spheres for emphasis. S0–S4 approximate the different binding sites. The arrows highlight the α -subunits in the flipped configuration.

showed that these mutations essentially stabilized the flipped configuration (Figure 2D–F and Movies 2–4 of the Supporting Information). T85M- and T85A-KcsA stabilized the flipped configuration for one of the α -subunits (Figure 2D,E), and G88R-KcsA stabilized the flipped configuration for two adjacent α -subunits (Figure 2F). The transition of the flipped carbonyl oxygen away from the central pore axis reflects a change in the dihedral angles around the V76–G77 amide plane. This can be visualized in an overlay of Ramachandran plots calculated at each picosecond of the simulation for the four α -subunits. Figure 3A shows the overlay of the Ramachandran plots for the WT-KcsA α -subunits. The dihedral angles for V76 and G77 are the most dynamic, which reflects the carbonyl oxygen alternating between the central pore axis

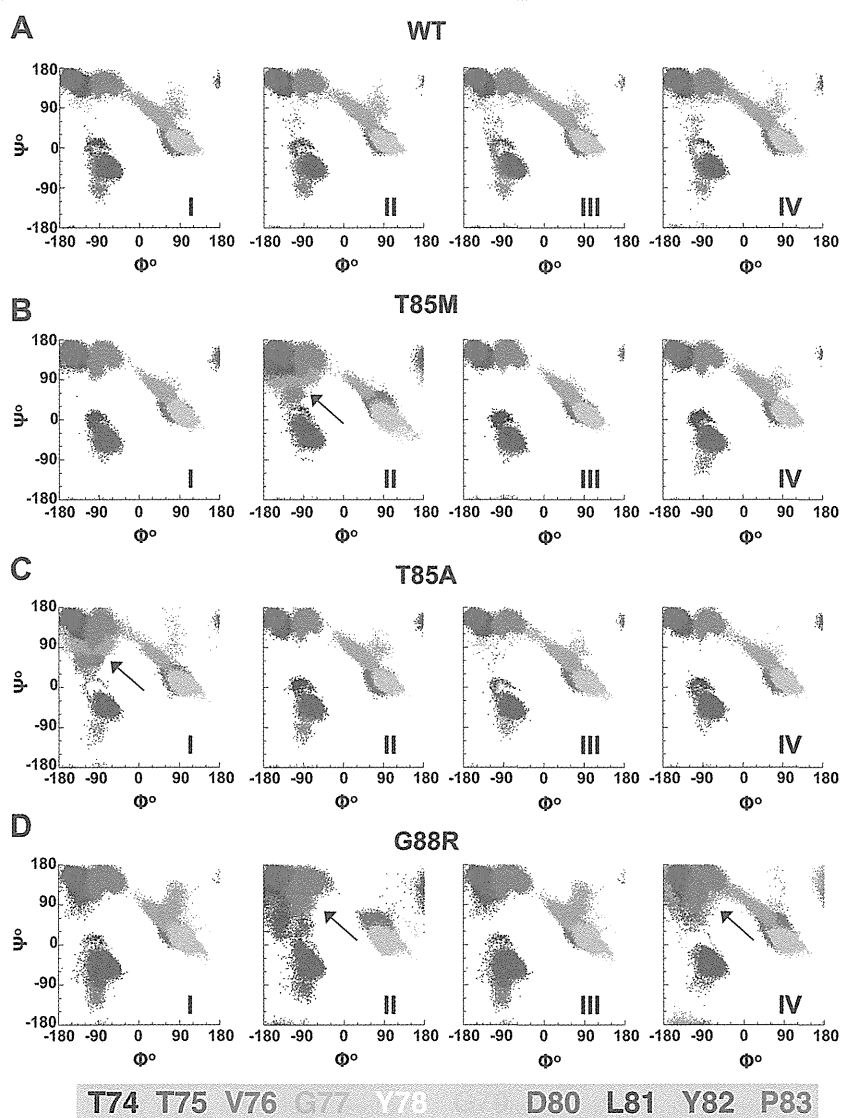


Figure 3. T85M-, T85A-, G88R-KcsA α -subunits in the flipped configuration disrupt the bond angle symmetry for the amino acid residues in the selectivity filter. An overlay of Ramachandran plots calculated at each picosecond from the trajectory file for the different selectivity filter amino acid residues (black for T74, brown for T75, red for V76, orange for G77, yellow for Y78, green for G79, blue for D80, violet for L81, purple for Y82, and gray for P83) for (A) WT-, (B) T85M-, (C) T85A-, or (D) G88R-KcsA α -subunits (I–IV). The arrows highlight the Ramachandran plots for the mutant α -subunits that have a stable flipped configuration.

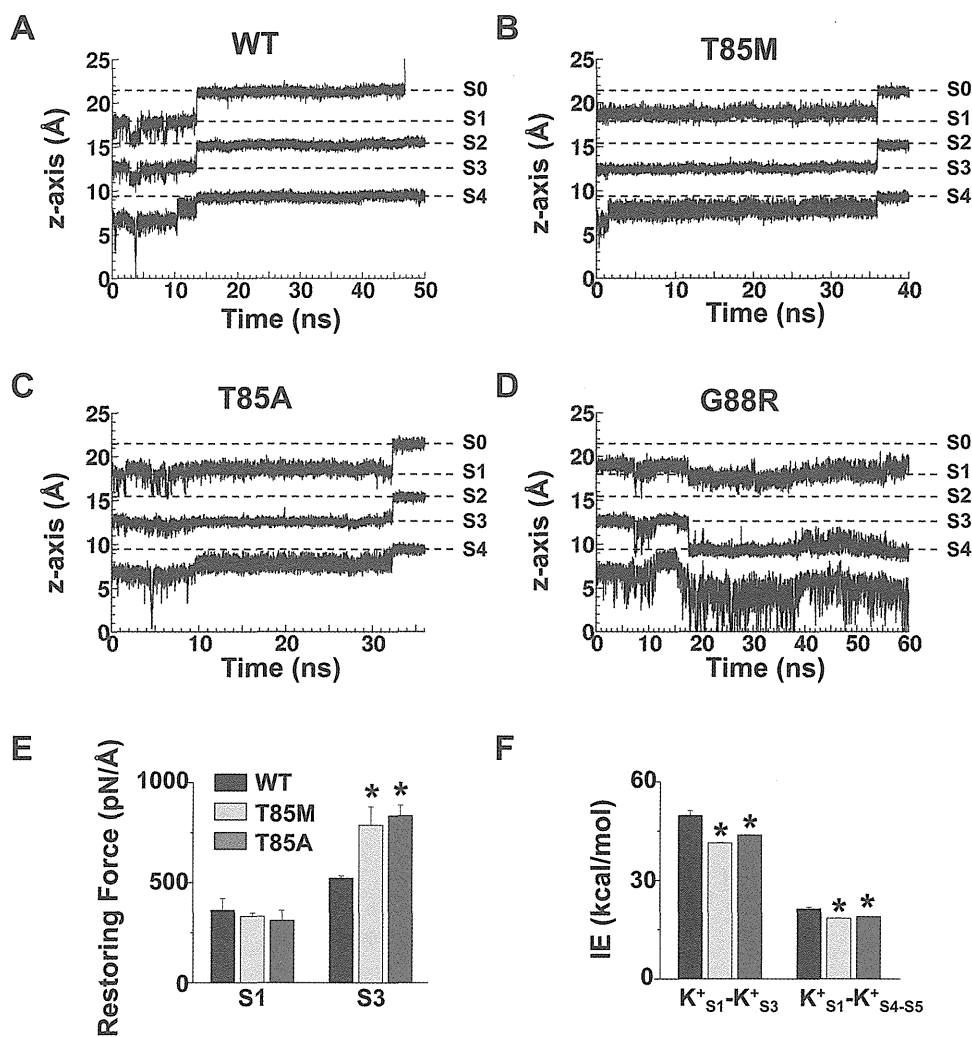


Figure 4. T85M-, T85A-, and G88R-KcsA mutations delay or disrupt the K⁺ permeation step, and T85M- and T85A-KcsA mutations increase the K⁺ restoring force at S3 and weaken K⁺-K⁺ repulsion at S1. (A–D) The graphs show the movement of the three K⁺ ions for (A) WT-, (B) T85M-, (C) T85A-, or (D) G88R-KcsA simulations along the z-axis over time. The origin for the z-coordinate is the center of the membrane (0 Å), and S0–S4 approximate the different binding sites from the WT-KcsA simulation. (E) The graph shows the mean restoring force calculated at S1 and S3 for WT-KcsA (black), T85M-KcsA (light gray), or T85A-KcsA (dark gray) ($n = 3$ simulations each) ($*p < 0.05$ compared to control). (F) The graph shows the mean interaction energies between the different K⁺ ions at S1 (K⁺_{S1}) or S3 (K⁺_{S3}) or the K⁺ ion moving into S4 (K⁺_{S4-S5}) for WT-KcsA (black), T85M-KcsA (light gray), or T85A-KcsA (dark gray) ($n = 3$ simulations each) ($*p < 0.05$ compared to control).

and flipped configuration. The Ramachandran plots for each WT-KcsA α -subunit are similar or symmetrical to one another. Panels B–D of Figure 3 show the Ramachandran plots for T85M-, T85A-, and G88R-KcsA, respectively. Notice the mutant α -subunits that stabilize the flipped configuration have very different Ramachandran plots when compared to the other α -subunits.

All the simulations were initiated with K⁺ ions at a weak binding site in the cavity (S5) and at S3–S1. The WT-KcsA simulation showed that the three K⁺ ions had moved from the initial (S5)–S3–S1 state to an S4–S2–(S0) state (Figure 2C). On the basis of the relative location of the K⁺ ions in the images from the mutant MDS (Figure 2D–F), the α -subunit(s) in the flipped configuration delayed the K⁺ ions from moving into the S4–S2–(S0) state. To better appreciate the dynamic movement of the different K⁺ ions during the simulations, we plotted

their z-axis coordinates over time (Figure 4). The WT-KcsA simulation showed that the K⁺ ion at S5 quickly approached S4, which was accompanied by the coordinated movement of the three K⁺ ions to the S4–S2–(S0) state (Figure 4A). This permeation step is qualitatively similar to the knock-on mechanism originally proposed by Hodgkin and Keynes³¹ and described in detail by Berneche and Roux for KcsA.¹⁵ The T85M- and T85A-KcsA simulations showed a similar permeation step but with a much longer delay (Figure 4B,C). Closer examination of the T85M- and T85A-KcsA simulations showed that the permeation could not occur as long as one of the α -subunits was in the flipped configuration. In contrast, the G88R-KcsA simulation showed dramatically different K⁺ ion trajectories (Figure 4D). The K⁺ ion at S5 approached S4 but then moved back into the cavity; the K⁺ ion at S3 then moved to S4, and the K⁺ ion at S1 stayed in place.

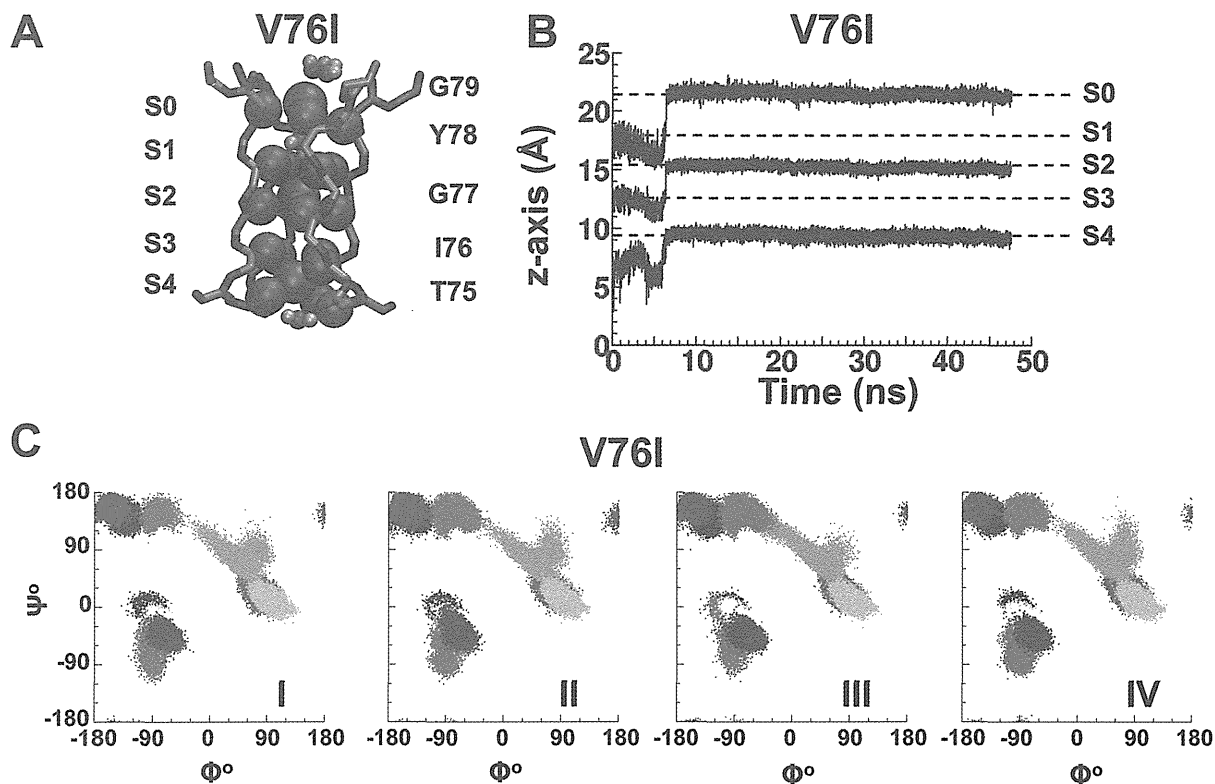


Figure 5. V76I-KcsA substitution that does not disrupt the binding sites in the selectivity filter or K^+ permeation. (A) Representative atomic image of the selectivity filter for V76I-KcsA. Shown are the TIGYG amino acid residues (light blue for C, red for O, and dark blue for N) for all four α -subunits, the bound K^+ ions (green), and several adjacent water molecules (red for O and gray for H). The oxygen atoms that line the filter and the K^+ ions are shown as large spheres, and water molecules are shown as small spheres for emphasis. S0–S4 approximate the different binding sites. (B) The graphs show the movement of the three K^+ ions along the z-axis over time. The origin for the z-coordinate axis is the center of the membrane, and S0–S4 approximate the different binding sites from the WT-KcsA simulation. V76I-KcsA does not delay or disrupt the permeation step. (C) Cumulative Ramachandran plots for the different selectivity filter amino acid residues (black for T74, brown for T75, red for I76, orange for G77, yellow for Y78, green for G79, blue for D80, violet for L81, purple for Y, and gray for P83) calculated for the four (I–IV) V76I-KcsA α -subunits. The Ramachandran plots for each V76I-KcsA α -subunit are similar to one another and to that of the WT-KcsA α -subunits (Figure 3A).

Because T85M- or T85A-KcsA delayed (but did not prevent) the permeation step, we speculated that they alter the relative attractive–repulsive forces that underlie rapid K^+ permeation. Accordingly, we calculated the change in the K^+ ion restoring force at S3 and the interaction energy (mainly Columbic repulsion) between the different K^+ ions (Figure 4E,F). When one of the α -subunits was in the flipped configuration, the K^+ ion at S3 interacted more closely with the remaining carbonyl oxygen atoms and the net electrostatic repulsion with the K^+ ion at S1 was decreased. Together, the data suggest that T85M- or T85A-KcsA upsets the balance of forces needed to facilitate that rapid exit of the K^+ ion at S1.

To ensure the robustness of the MDS, we performed a negative control by testing a substitution in the KcsA selectivity filter that is not expected to negatively affect K^+ permeation. V76 in the KcsA selectivity filter corresponds to I313 in the Kv7.1 (Figure 2A). This is a very conservative substitution whose side chain differs by only one methylene group, and functional studies show that the engineered I313V-Kv7.1 mutant is not different when compared to WT-Kv7.1.³² MDS of V76I-KcsA demonstrated it behaved like WT-KcsA (Figure 5A–C).

DISCUSSION

A major challenge for clinicians is to determine which therapeutic strategy is the most appropriate for an individual LQT1 patient. The value of genetic testing in selecting the proper therapy for a given patient is limited because of its inability to predict functional phenotypes accurately or forecast disease expressivity and/or severity. In an effort to move beyond genotype risk stratification simply based on the type of LQTS (i.e., LQT1, LQT2, LQT3, etc.), multiple studies are identifying intragenic approaches to correlate the risk for LQT-related cardiac events based on the type, location, and dysfunction of a mutation.^{9,13,33–35} These types of studies found that LQT1 mutations that disrupt conserved amino acids in the pore region are an independent risk factor for cardiac events.¹³ The purpose of this work was to provide molecular insight into how these high-risk LQT1 mutations might cause channels to malfunction. We were able to generate a robust molecular model for high-risk LQT1 mutations by (1) identifying a number of different LQT1 patients with the same mutations in the pore, (2) studying their functional phenotypes in vitro, and (3) performing MDS of analogous mutations in KcsA. The clinical data confirmed that these mutations conferred a high risk for LQT1-related events, and

the *in vitro* data suggested that mutations generate nonfunctional Kv7.1 channels and dominant negative effects. The *in silico* data suggested a mechanism for the disruption of channel function, namely, that a backbone conformational change disrupts permeation through the selectivity filter.

A major advantage in studying the LQT1 mutations using KcsA is that an effective model for K⁺ permeation has been developed for this structure.¹⁵ MDS that calculated the energetics of KcsA permeation suggest that the movement of K⁺ ions between binding sites in the selectivity filter is essentially barrierless; however, the K⁺ ion at S1 is in a deep energy well and cannot exit toward S0.^{15,19} Berneche and Roux proposed that this is overcome by electrostatic repulsion between the other K⁺ ions in the pore. As the K⁺ ion at S5 approaches S4, the second K⁺ ion at S3 initiates its transition to S2, and electrostatic repulsion from the incoming K⁺ ion at S4 and the K⁺ ion transiting to S2 lift the bottom of the deep free energy well for the K⁺ ion at S1. Ultimately, the K⁺ ion at S1 becomes unstable and exits toward S0. Without the repulsion from the other two incoming ions, the K⁺ ion at S1 remains trapped in its deep energy well.

The K⁺ trajectories for our WT-KcsA MDS are in good agreement with this energetic model of K⁺ permeation (Figure 4A). We found that incorporating T85M- and T85A-KcsA mutations primarily altered the S2–S3 binding site and decreased the net electrostatic repulsion from the incoming K⁺ ion at S4 and the ion at S3 (Figure 4F). The simulations suggested that this would increase the level of trapping of the K⁺ ion at S1 (Figure 4B,C) and decrease the level of K⁺ permeation. The effect that G88R-KcsA had on the S2–S3 binding site was much more severe and appeared to prevent the permeation step altogether.

The modeling raises several questions, including how different mutations stabilize the flipped configuration and why this is seen for one or more of the α -subunits. The simulations showed that T85M-, T85A-, and G88R-KcsA similarly potentiated the formation of hydrogen bonds between D80 and the R89 residue on the adjacent α -subunit (Figure 2B). We speculate the potentiation of this bond might increase the stability of the flipped configuration. The simulations also showed that when one of the T85M- or T85A-KcsA α -subunits entered the flipped configuration, the K⁺ ion at S3 more closely associated with the remaining carbonyl oxygen atoms (Figure 44E, movies 2,3 of the Supporting Information). This likely prevented the remaining α -subunits from entering the flipped configuration. However, if the K⁺ ion binding to S3 is lost, as it was in the G88R-KcsA simulation, then we suspect that all four of the α -subunits would eventually enter the flipped configuration. Indeed, not only a second but a third G88R-KcsA α -subunit entered the flipped configuration after 55 ns (data not shown).

There are several limitations to our approach. The functional data were obtained in a widely used heterologous expression system and may not completely recapitulate the native condition. Although the availability of a high-quality structure for the closely related KcsA allowed us to investigate the molecular basis for the functional disruption by the different LQT1 mutations, not all of the KcsA pore residues are identical to Kv7.1. To circumvent this, we attempted to perform MDS using a published Kv7.1 homology model. However, this proved to be problematic because the selectivity filter was unstable and required the application of dihedral restraints to support permeation (data not shown).³⁶ A more recent Kv7.1

homology model also proved to be problematic because the selectivity filter is in a C-type inactivated configuration.³⁷ A second limitation to using KcsA is that it does not include the obligatory I_{Ks} β -subunit KCNE1. KCNE1 profoundly affects Kv7.1 by eliminating C-type inactivation.^{38–41} Studies suggest that KCNE1 eliminates C-type inactivation by interacting with a phenylalanine (F340) in the second transmembrane segment of the pore domain, near the hinge region responsible for opening the channel. This phenylalanine is conserved in KcsA (F103),⁴² and studies indicate that, as KcsA opens, F103 reorients to form a hydrogen bond network in the selectivity filter to facilitate C-type inactivation.^{43,44} The interplay between KcsA opening and C-type inactivation is expected to occur in other K⁺ channels, including Kv7.1.^{42–44} Assuming KCNE1 prevents the reorientation of F340 in Kv7.1 to eliminate C-type inactivation, then the closed KcsA structure (which has F103 in an orientation that does not promote C-type inactivation) might represent an adequate surrogate to model the selectivity filter of a KCNE1-modified Kv7.1 channel. Lastly, MDS using KcsA do not provide mechanistic insight into how the mutations alter the cell surface membrane expression of Kv7.1 or its voltage-dependent gating. On the basis of the functional data, these changes do not likely account for the high-risk phenotypes in the patients. The level of cell surface expression of Kv7.1 was not decreased under conditions that mimicked heterozygosity (Figure 1B of the Supporting Information), and there are only relatively weak effects on gating (Table 2 of the Supporting Information).

In summary, we identified atomic-scale changes associated with higher-risk, dominant negative, pore-localizing LQT1-causative mutations. These data support the notion that MDS may assist in the pathogenic assessment of high-risk LQT1 mutations. We expect that subsequent advances in crystallography and homology modeling and improvements in the force field and computer hardware for MDS will further the applicability of this approach to nonconserved residues, other regions of Kv7.1, and other processes disrupted by LQT1 mutations (i.e., gating, co-assembly, phosphorylation, etc.).

■ ASSOCIATED CONTENT

📄 Supporting Information

Supplemental experimental procedures, Figure 1, Movies 1–4, and Tables 1 and 2. This material is available free of charge via the Internet at <http://pubs.acs.org>.

■ AUTHOR INFORMATION

Corresponding Author

*Address: 800 Rose St., MSS08, Lexington, KY 40536. Telephone: (859) 323-2797. Fax: (859) 323-1070. E-mail: brian.delisle@uky.edu.

Funding

This work was supported by American Heart Association Predoctoral Award PRE7370003 (D.C.B.) and National Heart, Lung and Blood Institute Grant R01 HL087039 (B.P.D.).

Notes

We declare the following competing financial interest(s): Dr. Michael J. Ackerman is a consultant for Biotronik, Boston Scientific, Medtronic, St. Jude Medical, and Transgenomic. In addition, there is a license agreement held between Transgenomic and Mayo Clinic Health Solutions, and royalties are distributed in accordance with Mayo Clinic policy.

■ ACKNOWLEDGMENTS

We acknowledge Dr. David Rodgers (University of Kentucky) for critical review of the manuscript, Eric S. Schmidt, McKenzie Johnson, and Jennifer L. Smith (University of Kentucky) for their technical assistance, and the University of Kentucky Information Technology department and Center for Computational Sciences for computing time on the Lipscomb High Performance Computing Cluster.

■ ABBREVIATIONS

LQTS, long QT syndrome; LQT1, type 1 long QT syndrome; MDS, molecular dynamics simulations; VMD, Visual Molecular Dynamics; NAMD, Not Just Another Molecular Dynamics program; POPC, palmitoyl-2-palmitoleoyl-*sn*-glycero-3-phosphocholine; rmsd, root-mean-square deviation.

■ REFERENCES

- (1) Ward, O. C. (1964) A New Familial Cardiac Syndrome in Children. *J. Ir. Med. Assoc.* 54, 103–106.
- (2) Romano, C. (1965) Congenital Cardiac Arrhythmia. *Lancet* 1, 658–659.
- (3) Lehnart, S. E., Ackerman, M. J., Benson, D. W., Jr., Brugada, R., Clancy, C. E., Donahue, J. K., George, A. L., Jr., Grant, A. O., Groff, S. C., January, C. T., Lathrop, D. A., Lederer, W. J., Makielski, J. C., Mohler, P. J., Moss, A., Nerbonne, J. M., Olson, T. M., Przywara, D. A., Towbin, J. A., Wang, L. H., and Marks, A. R. (2007) Inherited arrhythmias: A National Heart, Lung, and Blood Institute and Office of Rare Diseases workshop consensus report about the diagnosis, phenotyping, molecular mechanisms, and therapeutic approaches for primary cardiomyopathies of gene mutations affecting ion channel function. *Circulation* 116, 2325–2345.
- (4) Kapplinger, J. D., Tester, D. J., Salisbury, B. A., Carr, J. L., Harris-Kerr, C., Pollevick, G. D., Wilde, A. A., and Ackerman, M. J. (2009) Spectrum and prevalence of mutations from the first 2,500 consecutive unrelated patients referred for the FAMILION long QT syndrome genetic test. *Heart Rhythm* 6, 1297–1303.
- (5) Wang, Q., Curran, M. E., Splawski, I., Burn, T. C., Millholland, J. M., VanRaay, T. J., Shen, J., Timothy, K. W., Vincent, G. M., de Jager, T., Schwartz, P. J., Toubin, J. A., Moss, A. J., Atkinson, D. L., Landes, G. M., Connors, T. D., and Keating, M. T. (1996) Positional cloning of a novel potassium channel gene: KVLQT1 mutations cause cardiac arrhythmias. *Nat. Genet.* 12, 17–23.
- (6) Chouabe, C., Neyroud, N., Guicheney, P., Lazdunski, M., Romey, G., and Barhanin, J. (1997) Properties of KvLQT1 K⁺ channel mutations in Romano-Ward and Jervell and Lange-Nielsen inherited cardiac arrhythmias. *EMBO J.* 16, 5472–5479.
- (7) Wollnik, B., Schroeder, B. C., Kubisch, C., Esperer, H. D., Wieacker, P., and Jentsch, T. J. (1997) Pathophysiological mechanisms of dominant and recessive KVLQT1 K⁺ channel mutations found in inherited cardiac arrhythmias. *Hum. Mol. Genet.* 6, 1943–1949.
- (8) Neyroud, N., Denjoy, I., Donger, C., Gary, F., Villain, E., Leenhardt, A., Benali, K., Schwartz, K., Coumel, P., and Guicheney, P. (1998) Heterozygous mutation in the pore of potassium channel gene KvLQT1 causes an apparently normal phenotype in long QT syndrome. *Eur. J. Hum. Genet.* 6, 129–133.
- (9) Chouabe, C., Neyroud, N., Richard, P., Denjoy, I., Hainque, B., Romey, G., Drici, M. D., Guicheney, P., and Barhanin, J. (2000) Novel mutations in KvLQT1 that affect I_{Ks} activation through interactions with I_{Ks}. *Cardiovasc. Res.* 45, 971–980.
- (10) Deschenes, D., Achari, S., Pouliot, V., Hegele, R., Krahn, A., Daleau, P., and Chahine, M. (2003) Biophysical characteristics of a new mutation on the KCNQ1 potassium channel (L251P) causing long QT syndrome. *Can. J. Physiol. Pharmacol.* 81, 129–134.
- (11) Ruan, Y., Liu, N., Napolitano, C., and Priori, S. G. (2008) Therapeutic strategies for long-QT syndrome: Does the molecular substrate matter? *Circ.: Arrhythmia Electrophysiol.* 1, 290–297.
- (12) Kapa, S., Tester, D. J., Salisbury, B. A., Harris-Kerr, C., Pungliya, M. S., Alders, M., Wilde, A. A., and Ackerman, M. J. (2009) Genetic testing for long-QT syndrome: Distinguishing pathogenic mutations from benign variants. *Circulation* 120, 1752–1760.
- (13) Jons, C., Moss, A. J., Lopes, C. M., McNitt, S., Zareba, W., Goldenberg, I., Qi, M., Wilde, A. A., Shimizu, W., Kanter, J. K., Towbin, J. A., Ackerman, M. J., and Robinson, J. L. (2009) Mutations in conserved amino acids in the KCNQ1 channel and risk of cardiac events in type-1 long-QT syndrome. *J. Cardiovasc. Electrophysiol.* 20, 859–865.
- (14) Doyle, D. A., Morais Cabral, J., Pfuetzner, R. A., Kuo, A., Gulbis, J. M., Cohen, S. L., Chait, B. T., and MacKinnon, R. (1998) The structure of the potassium channel: Molecular basis of K⁺ conduction and selectivity. *Science* 280, 69–77.
- (15) Berneche, S., and Roux, B. (2001) Energetics of ion conduction through the K⁺ channel. *Nature* 414, 73–77.
- (16) Shrivastava, I. H., and Sansom, M. S. (2000) Simulations of ion permeation through a potassium channel: Molecular dynamics of KcsA in a phospholipid bilayer. *Biophys. J.* 78, 557–570.
- (17) Berneche, S., and Roux, B. (2000) Molecular dynamics of the KcsA K⁺ channel in a bilayer membrane. *Biophys. J.* 78, 2900–2917.
- (18) Jensen, M. O., Borhani, D. W., Lindorff-Larsen, K., Maragakis, P., Jogini, V., Eastwood, M. P., Dror, R. O., and Shaw, D. E. (2010) Principles of conduction and hydrophobic gating in K⁺ channels. *Proc. Natl. Acad. Sci. U.S.A.* 107, 5833–5838.
- (19) Bastug, T., and Kuyucak, S. (2011) Comparative study of the energetics of ion permeation in Kv1.2 and KcsA potassium channels. *Biophys. J.* 100, 629–636.
- (20) Berneche, S., and Roux, B. (2003) A microscopic view of ion conduction through the K⁺ channel. *Proc. Natl. Acad. Sci. U.S.A.* 100, 8644–8648.
- (21) Berneche, S., and Roux, B. (2005) A gate in the selectivity filter of potassium channels. *Structure* 13, 591–600.
- (22) Bastug, T., and Kuyucak, S. (2009) Importance of the peptide backbone description in modeling the selectivity filter in potassium channels. *Biophys. J.* 96, 4006–4012.
- (23) Choi, G., Kopplin, L. J., Tester, D. J., Will, M. L., Haglund, C. M., and Ackerman, M. J. (2004) Spectrum and frequency of cardiac channel defects in swimming-triggered arrhythmia syndromes. *Circulation* 110, 2119–2124.
- (24) Napolitano, C., Priori, S. G., Schwartz, P. J., Bloise, R., Ronchetti, E., Nastoli, J., Bottelli, G., Cerrone, M., and Leonardi, S. (2005) Genetic testing in the long QT syndrome: Development and validation of an efficient approach to genotyping in clinical practice. *JAMA, J. Am. Med. Assoc.* 294, 2975–2980.
- (25) Amin, A. S., Giudicessi, J. R., Tijssen, A. J., Spanjaart, A. M., Reckman, Y. J., Klemens, C. A., Tanck, M. W., Kapplinger, J. D., Hofman, N., Sinner, M. F., Muller, M., Wijnen, W. J., Tan, H. L., Bezzina, C. R., Creemers, E. E., Wilde, A. A., Ackerman, M. J., and Pinto, Y. M. (2012) Variants in the 3' untranslated region of the KCNQ1-encoded Kv7.1 potassium channel modify disease severity in patients with type 1 long QT syndrome in an allele-specific manner. *Eur. Heart J.* 33, 714–723.
- (26) Bartos, D. C., Duchatelet, S., Burgess, D. E., Klug, D., Denjoy, I., Peat, R., Lupoglazoff, J. M., Fressart, V., Berthet, M., Ackerman, M. J., January, C. T., Guicheney, P., and Delisle, B. P. (2011) R231C mutation in KCNQ1 causes long QT syndrome type 1 and familial atrial fibrillation. *Heart Rhythm* 8, 48–55.
- (27) Zhou, Y., Morais-Cabral, J. H., Kaufman, A., and MacKinnon, R. (2001) Chemistry of ion coordination and hydration revealed by a K⁺ channel-Fab complex at 2.0 Å resolution. *Nature* 414, 43–48.
- (28) Humphrey, W., Dalke, A., and Schulten, K. (1996) VMD: Visual molecular dynamics. *J. Mol. Graphics* 14, 27–38.
- (29) Phillips, J. C., Braun, R., Wang, W., Gumbart, J., Tajkhorshid, E., Villa, E., Chipot, C., Skeel, R. D., Kale, L., and Schulten, K. (2005) Scalable molecular dynamics with NAMD. *J. Comput. Chem.* 26, 1781–1802.
- (30) Goldenberg, I., Moss, A. J., Peterson, D. R., McNitt, S., Zareba, W., Andrews, M. L., Robinson, J. L., Locati, E. H., Ackerman, M. J.,

Benhorin, J., Kaufman, E. S., Napolitano, C., Priori, S. G., Qi, M., Schwartz, P. J., Towbin, J. A., Vincent, G. M., and Zhang, L. (2008) Risk factors for aborted cardiac arrest and sudden cardiac death in children with the congenital long-QT syndrome. *Circulation* 117, 2184–2191.

(31) Hodgkin, A. L., and Keynes, R. D. (1955) The potassium permeability of a giant nerve fibre. *J. Physiol.* 128, 61–88.

(32) Ikrar, T., Hanawa, H., Watanabe, H., Aizawa, Y., Ramadan, M. M., Chinushi, M., and Horie, M. (2009) Evaluation of channel function after alteration of amino acid residues at the pore center of KCNQ1 channel. *Biochem. Biophys. Res. Commun.* 378, 589–594.

(33) Zareba, W., Moss, A. J., Sheu, G., Kaufman, E. S., Priori, S., Vincent, G. M., Towbin, J. A., Benhorin, J., Schwartz, P. J., Napolitano, C., Hall, W. J., Keating, M. T., Qi, M., Robinson, J. L., and Andrews, M. L. (2003) Location of mutation in the KCNQ1 and phenotypic presentation of long QT syndrome. *J. Cardiovasc. Electrophysiol.* 14, 1149–1153.

(34) Shimizu, W., Horie, M., Ohno, S., Takenaka, K., Yamaguchi, M., Shimizu, M., Washizuka, T., Aizawa, Y., Nakamura, K., Ohe, T., Aiba, T., Miyamoto, Y., Yoshimasa, Y., Towbin, J. A., Priori, S. G., and Kamakura, S. (2004) Mutation site-specific differences in arrhythmic risk and sensitivity to sympathetic stimulation in the LQT1 form of congenital long QT syndrome: multicenter study in Japan. *J. Am. Coll. Cardiol.* 44, 117–125.

(35) Moss, A. J., Shimizu, W., Wilde, A. A., Towbin, J. A., Zareba, W., Robinson, J. L., Qi, M., Vincent, G. M., Ackerman, M. J., Kaufman, E. S., Hofman, N., Seth, R., Kamakura, S., Miyamoto, Y., Goldenberg, L., Andrews, M. L., and McNitt, S. (2007) Clinical aspects of type-1 long-QT syndrome by location, coding type, and biophysical function of mutations involving the KCNQ1 gene. *Circulation* 115, 2481–2489.

(36) Smith, J. A., Vanoye, C. G., George, A. L., Jr., Meiler, J., and Sanders, C. R. (2007) Structural models for the KCNQ1 voltage-gated potassium channel. *Biochemistry* 46, 14141–14152.

(37) Strutz-Seebohm, N., Pusch, M., Wolf, S., Stoll, R., Tapken, D., Gerwert, K., Attali, B., and Seebohm, G. (2011) Structural basis of slow activation gating in the cardiac I_{Ks} channel complex. *Cell. Physiol. Biochem.* 27, 443–452.

(38) Barhanin, J., Lesage, F., Guillemare, E., Fink, M., Lazdunski, M., and Romey, G. (1996) K(V)LQT1 and IsK (minK) proteins associate to form the I(Ks) cardiac potassium current. *Nature* 384, 78–80.

(39) Sanguinetti, M. C., Curran, M. E., Zou, A., Shen, J., Spector, P. S., Atkinson, D. L., and Keating, M. T. (1996) Coassembly of K(V)LQT1 and minK (IsK) proteins to form cardiac I(Ks) potassium channel. *Nature* 384, 80–83.

(40) Panaghie, G., Tai, K. K., and Abbott, G. W. (2006) Interaction of KCNE subunits with the KCNQ1 K⁺ channel pore. *J. Physiol.* 570, 455–467.

(41) Panaghie, G., Purtell, K., Tai, K. K., and Abbott, G. W. (2008) Voltage-dependent C-type inactivation in a constitutively open K⁺ channel. *Biophys. J.* 95, 2759–2778.

(42) McCoy, J. G., and Nimigeon, C. M. (2012) Structural correlates of selectivity and inactivation in potassium channels. *Biochim. Biophys. Acta* 1818, 272–285.

(43) Cuello, L. G., Jogini, V., Cortes, D. M., Pan, A. C., Gagnon, D. G., Dalmas, O., Cordero-Morales, J. F., Chakrapani, S., Roux, B., and Perozo, E. (2010) Structural basis for the coupling between activation and inactivation gates in K⁺ channels. *Nature* 466, 272–275.

(44) Cuello, L. G., Jogini, V., Cortes, D. M., and Perozo, E. (2010) Structural mechanism of C-type inactivation in K⁺ channels. *Nature* 466, 203–208.



Drug-induced QT-interval prolongation and recurrent torsade de pointes in a child with heterotaxy syndrome and *KCNE1* D85N polymorphism^{☆,☆☆}

Lisheng Lin, MD,^{a,*} Hitoshi Horigome, MD, PhD,^a Naoko Nishigami, MD,^a Seiko Ohno, MD, PhD,^b Minoru Horie, MD, PhD,^b Ryo Sumazaki, MD, PhD^a

^a Department of Child Health, Graduate School of Comprehensive Human Sciences, University of Tsukuba, Ibaraki, Japan

^b Department of Cardiovascular and Respiratory Medicine, Shiga University of Medical Science, Shiga, Japan

Received 18 June 2012

Abstract

We present a child case of heterotaxy syndrome (asplenia syndrome) after Fontan procedure that showed extreme prolongation of QT interval and torsade de pointes (TdP) after administration of sodium channel blockers for paroxysmal atrial tachycardia. Despite low serum concentration of the drugs, QT prolongation persisted and TdP attacks with unconsciousness recurred, possibly in association with junctional bradycardia and myocardial damage although he had never experienced QT prolongation during bradycardia before. Temporal cardiac pacing via a venous route to exclude possible implication of bradycardia in induction of TdP was difficult to apply due to total cavopulmonary connection (TCPC) circulation. Continuous intravenous administration of low-dose isoproterenol was started but an appropriate heart rate for prevention of TdP was difficult to obtain. Finally, we were urged to conduct implantation of a DDD pacemaker combined with ICD surgically with epicardial leads, resulting in successful suppression of TdP and syncope. Screening of the genotype disclosed the *KCNE1* D85N polymorphism, which is known as one of the typical disease-causing gene variants in long-QT syndrome (LQTS).

© 2012 Elsevier Inc. All rights reserved.

Keywords:

Drug-induced long-QT syndrome; Torsade de pointes; *KCNE1* D85N; Sodium channel blocker

Introduction

Antiarrhythmic agents are known to potentially cause QT-interval prolongation and torsade de pointes (TdP), i.e., drug-induced long-QT syndrome (di-LQTS). Recent advancements in molecular biology have revealed that genetic background is often implicated in this life-threatening proarrhythmia.¹ Here, we present a child case of heterotaxy syndrome (asplenia syndrome) after Fontan procedure that showed extreme prolongation of QT interval and recurrent TdP after administration of sodium channel blockers for paroxysmal atrial tachycardia. Screening of the genotype disclosed the *KCNE1* D85N polymorphism, which is known as one of the typical disease-causing gene variants in LQTS.²

Case report

A 15-year-old boy was admitted to our hospital because of palpitations. The patient had been diagnosed with heterotaxy syndrome, single atrium, double-inlet single ventricle, pulmonary arterial stenosis, and total anomalous pulmonary venous return (TAPVR), and had undergone total cavopulmonary connection (TCPC) with an extra cardiac conduit combined with TAPVR repair. Electrocardiogram (ECG) on admission revealed atrial tachycardia (AT) with 1:1 atrioventricular conduction (heart rate 150 bpm) although the patient had not previously shown significant arrhythmias, except for transient asymptomatic junctional or sinus bradycardia probably associated with heterotaxy with a heart rate of around 50–60 bpm (Fig. 1). He was hemodynamically stable and medical therapies were started. Repeated intravenous injections of ATP (maximum dose, 0.25 mg/kg) and procainamide (5 mg/kg) failed to convert AT into sinus rhythm. Then, intravenous disopyramide (1 mg/kg) was administered. Eight minutes after the infusion, pulseless tachycardia was suddenly provoked, and a DC shock was applied, resulting in successful conversion. However, AT recurred shortly and therefore continuous infusion of low doses of landiolol (3 µg/kg/min)

[☆] This study was conducted at the University of Tsukuba.

^{☆☆} Grants or financial support for this work: None.

* Corresponding author. Department of Child Health, Graduate School of Comprehensive Human Sciences, University of Tsukuba, 1-1-1 Tenodai, Tsukuba 305-8575, Japan.

E-mail address: lishenglin5433@gmail.com

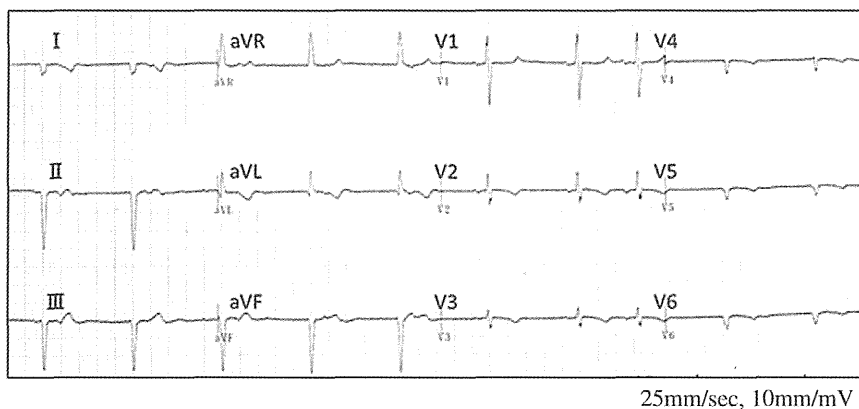


Fig. 1. Baseline 12-lead ECG recorded 3 months before admission, showing junctional bradycardia with a normal QT interval (heart rate 60bpm, QTc 400ms).

and digoxin (0.005 mg/kg, twice a day) were started, in order to control the heart rate and to prevent circulatory collapse by recurrence of AT/tachycardia. AT was then under controlled but bradycardia developed gradually and remarkable QT-interval prolongation ($QTc \geq 580$ ms) with frequent premature ventricular contraction appeared on ECG monitoring (Fig. 2A and B). Serum levels of potassium, calcium and magnesium were all normal. Although all antiarrhythmic drugs were discontinued, extreme QT prolongation persisted and TdP attacks with unconsciousness recurred (Fig. 2C), necessitating DC shocks several times.

Because immediate application of temporal cardiac pacing via a venous route to exclude possible implication of bradycardia in induction of TdP was difficult to apply due to TCPC circulation, we tried continuous intravenous administration of low doses of isoproterenol. However, an appropriate heart rate for the prevention of TdP was difficult to obtain and a storm of TdP attacks reoccurred. Serum concentration of both procainamide and disopyramide later turned out to be low (0.7 and 0.3 $\mu\text{g/ml}$ at 12 h and 0.5 and, $<0.1 \mu\text{g/ml}$ at 36 h after administration, respectively) compared with their therapeutic ranges (4–10 and 2.8–3.2 $\mu\text{g/ml}$, respectively). Ultimately, 60 h after admission, we were urged to conduct implantation of a DDD pacemaker combined with ICD surgically with epicardial leads, resulting in successful suppression of TdP and syncope.

A genetic test for LQTS candidate genes revealed the *KCNE1* D85N polymorphism in the index case and in his father (Fig. 3). His mother was negative for the single nucleotide polymorphism (SNP).

Discussion

The present case demonstrated that, even with low serum concentration of sodium channel blocker, marked QT prolongation and recurrent TdP can occur if the patient has other coexistent predisposing factors such as polymorphisms in the LQTS-related genes, as well as bradycardia. Ackerman et al.³ reported that the allele frequency of the *KCNE1* D85N polymorphism, which was detected in the present case, is approximately 0.7% in healthy Asian populations. According to the survey conducted by Nishio et al.² in Japan, its

frequency among LQTS probands (3.9%) is significantly higher than that in healthy control subjects (0.81%). This gene polymorphism has recently gathered much interest as a typical culprit of unexpected sudden cardiac death or aborted cardiac death as well as di-LQTS.⁴ In an experiment using *Xenopus* oocytes, I_{Ks} currents were reduced by approximately 50% under heterologous expression of the D85N gene variant.⁵ Another functional analysis study using hamster ovarian cells showed that I_{Ks} and I_{Kr} currents of those with the D85N gene variant were reduced by 28% and 31%–36%, respectively.²

Sodium channel blocker is one of the most common antiarrhythmic agents used for treatment of tachyarrhythmias. On the other hand, it is also known as one of the typical drugs that provoke di-LQTS/TdP.¹ Sodium channel blocker prolongs both myocardial depolarization and repolarization especially in ischemic or injured regions, enhancing electrical dispersion of myocardium. In the present case, it is difficult to conclude that the significant QT-interval prolongation was caused by *KCNE1* D85N alone. Implication of heterotaxy-related junctional or sinus bradycardia at baseline or some kind of myocardial damage such as clinically unapparent myocarditis in the development of LQT/TdP could not be fully excluded. However, it is unlikely that the latter mechanism alone induced LQT/TdP because the patient had never shown prolonged QT or symptomatic arrhythmias previously even during the phase of marked bradycardia or hemodynamic instability around surgical procedure. It is considered reasonable that *KCNE1* D85N played a significant role as genetic background for development of the life-threatening event in this patient. However, this genetic variance does not seem to have any pathophysiologic relevance to heterotaxy syndrome because we are not aware of any case reports that indicate such association in the literature.

It should be noted that a transvenous approach for temporal pacing is not easy in patients with complex heart disease who have already undergone TCPC in spite of the fact that heterotaxia hearts are often complicated by supraventricular tachycardia, necessitating the use of anti-tachycardia drugs.⁶ If a patient with heterotaxy shows episodes of sustained tachycardia, electrophysiological study and catheter ablation of the foci of tachycardia, if necessary, should be conducted before Fontan procedure.

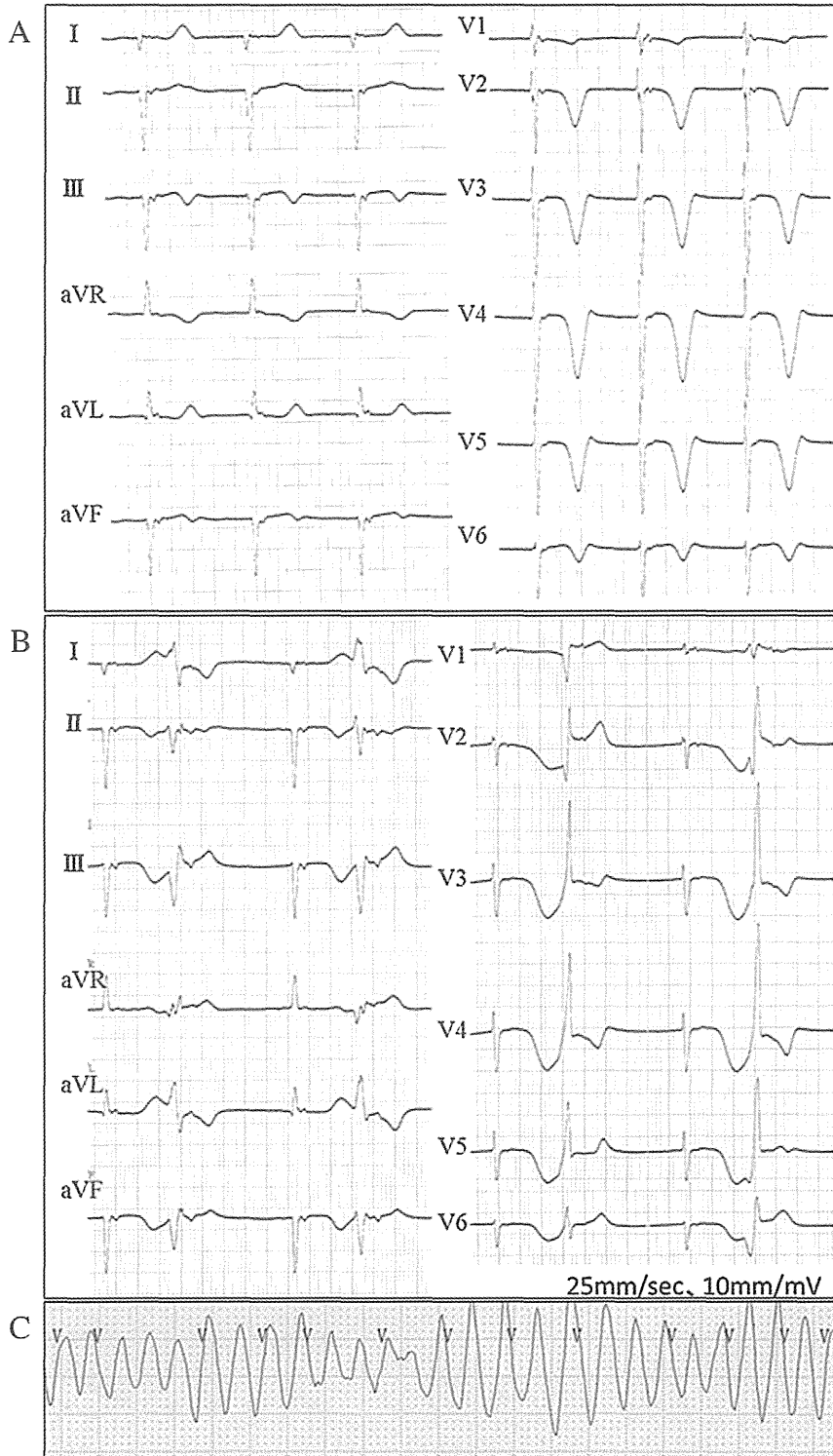


Fig. 2. A: ECG recorded 11h after administration of sodium channel blockers, showing marked QT-interval prolongation with bradycardia (heart rate 60bpm, QTc 580ms). B: ECG showing marked QT-interval prolongation and bigeminy of premature ventricular contraction. C: TdP following extreme QT prolongation.

KCNE1

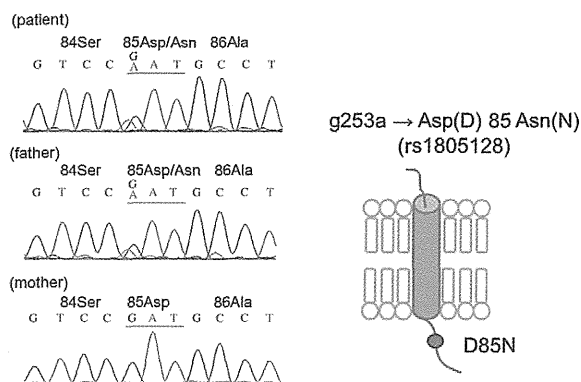


Fig. 3. Representation of direct sequencing of the *KCNE1* of the patient and parents. A G to A transition at codon 253 and resultant amino acid substitution of asparagine for aspartic acid were detected in the index patient and father.

References

1. Itoh H, Sakaguchi T, Ding WG, et al. Latent genetic backgrounds and molecular pathogenesis in drug-induced long-QT syndrome. *Circ Arrhythm Electrophysiol* 2009;2:511.
2. Nishio Y, Makiyama T, Itoh H, et al. D85N, a *KCNE1* polymorphism, is a disease-causing gene variant in long QT syndrome. *J Am Coll Cardiol* 2009;54:812.
3. Ackerman MJ, Tester DJ, Jones GS, Will ML, Burrow CR, Curran ME. Ethnic differences in cardiac potassium channel variants: implications for genetic susceptibility to sudden cardiac death and genetic testing for congenital long QT syndrome. *Mayo Clin Proc* 2003;78:1479.
4. Paulussen AD, Gilissen RA, Armstrong M, et al. Genetic variations of *KCNQ1*, *KCNH2*, *SCN5A*, *KCNE1*, and *KCNE2* in drug-induced long QT syndrome patients. *J Mol Med* 2004;82:182.
5. Westenskow P, Splawski I, Timothy KW, Keating MT, Sanguinetti MC. Compound mutations: a common cause of severe long-QT syndrome. *Circulation* 2004;109:1834.
6. Miyazaki A, Sakaguchi H, Ohuchi H, et al. The clinical course and incidence of supraventricular tachyarrhythmias after extra-cardiac conduit Fontan procedures in relation to atrial situs. *Circ J* 2011; 75:413.

Phenotype Variability in Patients Carrying *KCNJ2* Mutations

Hiromi Kimura, MD; Jun Zhou, PhD; Mihoko Kawamura, MD; Hideki Itoh, MD, PhD;
Yuka Mizusawa, MD; Wei-Guang Ding, MD, PhD; Jie Wu, PhD; Seiko Ohno, MD, PhD;
Takeru Makiyama, MD, PhD; Akashi Miyamoto, MD, PhD; Nobu Naiki, MD; Qi Wang, BS;
Yu Xie, BS; Tsugutoshi Suzuki, MD, PhD; Shigeru Tateno, MD, PhD;
Yoshihide Nakamura, MD, PhD; Wei-Jin Zang, PhD; Makoto Ito, MD, PhD;
Hiroshi Matsuura, MD, PhD; Minoru Horie, MD, PhD

Background—Mutations of *KCNJ2*, the gene encoding the human inward rectifier potassium channel Kir2.1, cause Andersen-Tawil syndrome (ATS), a disease exhibiting ventricular arrhythmia, periodic paralysis, and dysmorphic features. However, some *KCNJ2* mutation carriers lack the ATS triad and sometimes share the phenotype of catecholaminergic polymorphic ventricular tachycardia (CPVT). We investigated clinical and biophysical characteristics of *KCNJ2* mutation carriers with “atypical ATS.”

Methods and Results—Mutational analyses of *KCNJ2* were performed in 57 unrelated probands showing typical (≥ 2 ATS features) and atypical (only 1 of the ATS features or CPVT) ATS. We identified 24 mutation carriers. Mutation-positive rates were 75% (15/20) in typical ATS, 71% (5/7) in cardiac phenotype alone, 100% (2/2) in periodic paralysis, and 7% (2/28) in CPVT. We divided all carriers ($n=45$, including family members) into 2 groups: typical ATS (A) ($n=21$, 47%) and atypical phenotype (B) ($n=24$, 53%). Patients in (A) had a longer QUC interval [(A): 695 ± 52 versus (B): 643 ± 35 ms] and higher U-wave amplitude (0.24 ± 0.07 versus 0.18 ± 0.08 mV). C-terminal mutations were more frequent in (A) (85% versus 38%, $P < 0.05$). There were no significant differences in incidences of ventricular tachyarrhythmias. Functional analyses of 4 mutations found in (B) revealed that R82Q, R82W, and G144D exerted strong dominant negative suppression (current reduction by 95%, 97%, and 96%, respectively, versus WT at -50 mV) and T305S moderate suppression (reduction by 89%).

Conclusions—*KCNJ2* gene screening in atypical ATS phenotypes is of clinical importance because more than half of mutation carriers express atypical phenotypes, despite their arrhythmia severity. (*Circ Cardiovasc Genet.* 2012; 5:344-353.)

Key Words: CPVT ■ ion channels ■ Andersen-Tawil syndrome ■ *KCNJ2* ■ phenotype

Andersen-Tawil syndrome (ATS) represents a disease entity characterized by 3 features: (1) ventricular arrhythmias with Q(T)U prolongation, (2) periodic paralysis, and (3) dysmorphic features.^{1,2} It is an autosomal-dominant inherited disease resulting from a heterozygous mutation of the *KCNJ2* gene. This gene encodes an inward rectifier K channel (Kir2.1), ubiquitously expressed in the myocardium, skeletal muscle, brain, and osteocytes.³ Since the first discovery of a mutation in this disease in 2001,⁴ we have extensively examined *KCNJ2* mutations in patients suspected of having ATS.⁵⁻⁷ In 2007, we described both the clinical and genetic

features of 23 patients (13 probands and 10 family members) and reported that the identification rate of *KCNJ2* mutation in this cohort was 100% if the patients satisfied ≥ 2 features of ATS.⁸ On a closer inspection, however, we noticed that $\approx 30\%$ of the *KCNJ2* mutation carriers lacked 2 of the ATS features: frequent PVC, bidirectional or polymorphic ventricular tachycardias (bVT or pVT), with QT or QU prolongation, without periodic paralysis or dysmorphic features. Recently, Tester et al⁹ reported a possible phenotypic overlap between ATS and catecholaminergic polymorphic VT (CPVT). CPVT is a form of inherited cardiac arrhythmia,

Received November 23, 2011; accepted April 18, 2012.

From the Department of Cardiovascular and Respiratory Medicine (H.K., J.Z., M.K., H.I., Y.M., J.W., S.O., A.M., N.N., Q.W., M.I., M.H.) and the Department of Physiology (W.-G.D., Y.X., H.M.), Shiga University of Medical Science, Otsu, Japan; the Department of Cardiovascular Medicine, Kyoto University Graduate School of Medicine, Kyoto, Japan (T.M.); the Department of Pediatric Electrophysiology, Osaka City General Hospital, Osaka, Japan (T.S.); the Department of Pediatrics, Chiba Cardiovascular Center, Ichihara, Japan (S.T.); the Department of Pediatrics, Kinki University Faculty of Medicine, Higashiosaka, Japan (Y.N.); and the Department of Pharmacology, Xi'an Jiaotong University, College of Medicine, Xi'an, China (J.Z., W.-J.Z.).

Correspondence to Minoru Horie, MD, PhD, Department of Cardiovascular and Respiratory Medicine, Shiga University of Medical Science, Seta-Tsukinowa, Otsu, Shiga, 520-2192 Japan. E-mail horie@belle.shiga-med.ac.jp

© 2012 American Heart Association, Inc.

Circ Cardiovasc Genet is available at <http://circgenetics.ahajournals.org>

DOI: 10.1161/CIRCGENETICS.111.962316

Downloaded from circgenetics.ahajournals.org by guest on June 19, 2012

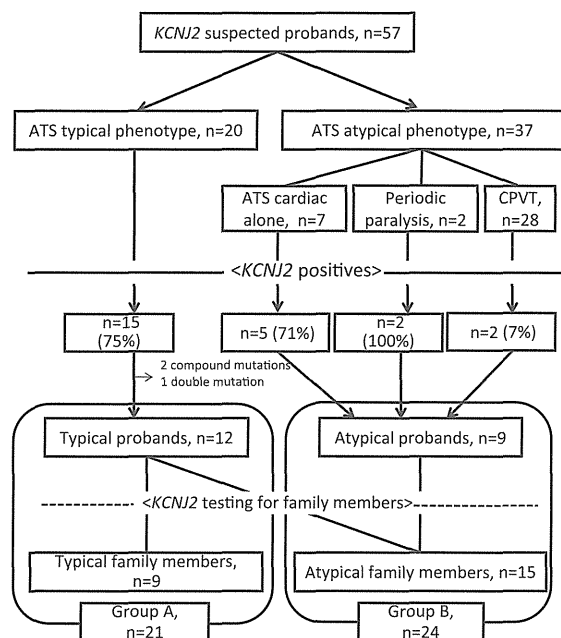


Figure 1. A Flow Chart of 57 probands suspected as carriers of *KCNJ2* mutations. ATS indicates Andersen-Tawil syndrome; CPVT, catecholaminergic polymorphic ventricular tachycardia.

characterized by exercise- and/or stress-induced p/bVTs with a normal cardiac structure.¹⁰ However, the incidence and clinical characteristics of atypical ATS and *KCNJ2*-related CPVT remain unknown.

Clinical Perspective on p 353

In the present study, we conducted the genetic screening for *KCNJ2* mutation-related phenotypes—those fulfilling at least 1 of the ATS features or CPVT criteria. We compared the clinical and genetic features between typical ATS and atypical phenotype (only 1 of the ATS features or CPVT) patients. We hypothesized that the mutated channel function found in patients with atypical ATS phenotypes would show different I_{K1} current properties. Using the patch-clamp technique, we examined the functional features of four mutations found in the atypical phenotype group.

Methods

Study Subjects

Fifty-seven unrelated probands (65% females, age at diagnosis: 18 ± 12 years old) from 31 institutes in Japan were enrolled in the study. They were clinically diagnosed with either typical ATS (defined as patients with ≥ 2 ATS features) ($n=20$), mild ATS [those with 1 of the ATS features—cardiac arrhythmia alone ($n=7$), periodic paralysis with an abnormal U wave ($n=2$)], or CPVT ($n=28$) (Figure 1 and Table 1).

Three features of ATS were clinically determined as follows: (1) Cardiac involvement was determined by the presence of ventricular arrhythmias (frequent premature ventricular contractions (PVCs), bigeminy, bVT, pVT, or monomorphic VT), with prolongation of the corrected QU interval and/or a prominent U wave. (2) The presence of periodic paralysis was based on standard criteria.¹¹ (3) Dysmorphic features were defined by the presence of 2 or more of the following: (a) low-set ears, (b) hypertelorism (wide-set eyes), (c) a small mandible, (d) clinodactyly (permanent lateral or medial curve of a finger or toe), and (e) syndactyly (persistent webbing between fingers or toes).¹²

Twenty-eight of the 57 patients fulfilled the diagnostic criteria of CPVT—exertional syncope plus documentation of bVT or pVT during exercise or exercise tests. Patients with QT prolongation were excluded.¹⁰

ECG Manifestation

We measured QU intervals if there was a prominent U wave and QT intervals in cases showing no U wave. The QT interval was defined from the onset of QRS to the end of the T wave. The U wave was defined as an early diastolic deflection after the end of the T wave. The QU interval was defined from the onset of QRS to the end of the U wave. QT and QU intervals were corrected according to the Bazett formula.^{13,14} The end of the T or U wave was the point at which a tangent drawn to the steepest portion of the terminal part of the T or U wave crossed the isoelectric line.¹⁵ Because a prominent U wave is often fused to the next PQ segment in some cases, we defined the isoelectric line as a segment connecting 2 points preceding consecutive QRS complexes. A diagnosis of QT prolongation was made if the QTc exceeded 440 ms for males and 460 ms for females, in accordance with the standard criteria.¹⁶ Abnormal U waves were judged based on the following criteria: (a) wave amplitude ≥ 0.2 mV or (b) amplitude larger than preceding T wave.^{8,17}

bVT was identified as a VT characterized by a beat-to-beat alternation of the QRS axis in most of the documented runs of ventricular tachycardia (>4 consecutive beats).¹⁰ pVT was defined as the VT with an irregularly variable axis of the QRS.

DNA Isolation and Mutation Analysis

The protocol for genetic analysis was approved by the institutional ethics committee and performed under its guidelines. All patients

Table 1. Demographic Characteristics of Different Patient Cohorts: *KCNJ2* Mutation Incidence Rates (57 Probands)

	Typical ATS (Group A)	Atypical ATS (Group B)			Total
		ATS Cardiac Alone	ATS Periodic Paralysis Alone	CPVT	
Probands, n	20	7	2	28	57
Female, n (%)	13 (65)	5 (71)	0	19 (68)	37 (65)
Age, y	17 ± 11	21 ± 13	19 ± 6	18 ± 13	18 ± 12
QT(U)c,* ms	660 ± 90	600 ± 106	548 ± 77	429 ± 65	
<i>KCNJ2</i> positives, n (%)	15 (75)	5 (71)	2 (100)	2 (7)	24 (42)

ATS indicates Andersen-Tawil syndrome; CPVT, catecholaminergic polymorphic ventricular tachycardia.
*QUc interval was used in typical ATS, ATS cardiac phenotype alone, and ATS periodic paralysis alone. QTc interval was used in CPVT.

Table 2. *KCNJ2* Mutation-Carrying Probands (n=24)

	Case No.	<i>KCNJ2</i> -DNA	Protein	Age/Sex	ECG†	QTc/QUc, ms	Dysmorphism	Paralysis	Mutated Channel Function‡	Syncope/ACA	Treatment
Typical ATS phenotype (n=15)	1	118C>T	R40X*	15/F	1, 2	451/618	+	–	–	–/–	BB
	2	200G>A	R67Q	14/F	1, 2	360/626	+	+	d.n. ⁸	–/–	lb, BB
	3	244C>T	R82W	11/M	2	NA/NA	+	–	d.n. ^{9,27}	–/–	BB
			KCNH2-P1093L								
	4	430G>A	G144S	32/F	1, 2	NA/NA	+	+	d.n. ^{8,12}	+/+	IV, BB
			KCNQ1-A341V								
	5	436G>A	G146S	27/F	2	487/731	NA	+	d.n. ⁸	–/–	BB
	6	574A>G	T192A	16/M	1	420/700	–	+	d.n. ⁵	–/–	Az
	7	653G>A	R218Q	13/F	2	423/741	–	+	d.n. ⁸	–/–	BB, Az
	8	653G>A	R218Q	12/F	2	434/616	+	+	d.n. ⁸	–/–	Az
	9	653G>A	R218Q	12/M	1, 4	483/716	+	–	d.n. ⁸	–/–	...
	10	652C>T	R218W	6/F	1	365/753	–	+	d.n. ^{4,8}	+/-	FL
	11	652C>T	R218W	11/F	3	508/701	+	–	d.n. ^{4,8}	–/–	lb, BB
	12	652C>T	R218W	6/M	2	NA/NA	+	+	d.n. ^{4,8}	–/–	IV
	13	652C>T	R218W	19/F	2	468/681	+	–	d.n. ^{4,8}	+/-	BB
14	652C>T	R218W	12/M	1, 2, 3	400/689	+	–	d.n. ^{4,8}	–/–	...	
15	238C>T	R80C*	5/M	1, 2	468/681	+	+	R80C: –	–/–	...	
	904G>A	V302 M						V302 M: d.n., tr ¹²			
ATS cardiac phenotype alone (n=5)	16	245G>A	R82Q	46/F	2, 6	553/680	–	–	d.n.	–/–	...
									Figures 4, 5		
	17	244C>T	R82W	29/F	1, 2	433/672	–	–	d.n. ^{9,27}	–/–	BB
									Figures 4, 5		
	18	652C>T	R218W	6/F	1, 3	427/617	–	–	d.n. ^{4,8}	–/–	BB
19	652C>T	R218W	5/M	1, 3	392/707	–	–	d.n. ^{4,8}	–/–	IV	
20	683ins§	R228ins*	24/M	1, 4	498/...	–	–	–	–/–	Pil	
Periodic paralysis alone	21	199C>T	R67W	24/M	...	425/625	–	+	d.n. ⁸	–/–	Az
	22	1106C>A	S369X	13/M	...	472/600	–	+	tr ⁷	–/–	...
CPVT	23	431G>A	G144D	32/F	3	465/NA	–	–	Figures 4, 5	+/+	BB, FL
	24	914C>G	T305S*	36/F	1, 4, 5	443/664	–	–	Figures 4, 5	+/+	BB, ICD

NA indicates not available; age, age at diagnosis; ACA, aborted cardiac arrest; CPVT, catecholaminergic polymorphic ventricular tachycardia; ICD, implantable cardioverter-defibrillator; BB, β -blocker; lb, mexiletine; IV, verapamil; FL, flecainide; Pil, pilsicainide; and Az, acetazolamide.

*Novel mutation.

†PVC=1, bVT=2, pVT=3, VT=4, ventricular fibrillation=5, long-QT=6.

‡d.n. indicates dominant negative; tr, trafficking defect.

§683insGAAAAGCCACTTGGTGAAGCTCATGTTCCG.

||R228insKSHLVEAHVR.

provided informed consent before the genetic analysis was carried out. Genomic DNA was isolated from leukocyte nuclei using a DNA purification kit (Maxwell Blood DNA Purification Kit, Promega, Madison, WI). Genetic screening was first performed using denaturing high-performance liquid chromatography (dHPLC WAVE System; Transgenomic, Omaha, NE).¹⁸ Abnormal conformers were amplified via PCR, and sequencing was performed on an ABI 3130 DNA sequencer (Perkin Elmer, Foster City, CA). The cDNA sequence numbering was based on the GenBank reference sequence NM_000891.2 for *KCNJ2*. Regarding suspected CPVT probands, we also performed screening involving target mutation analysis for 34 *RyR2* gene exons (3, 8–16, 44–49, 83–84, 88–89, 91–97, and 99–105)^{19,20} and all exons of the *CASQ2* gene. In addition to these 3 genes, we examined the entire coding sequence of *KCNQ1*, *KCNH2*, *SCN5A*, and *KCNE1-5* to exclude the unexpected presence of compound mutations related to primary electric diseases.^{21,22} When a mutation was detected, we examined its presence in >200

Japanese control subjects to exclude the possibility of polymorphisms. When mutations were detected in probands, we also screened their family members.

Genotype-Phenotype Correlation

Baseline clinical characteristics collected were the age at diagnosis, symptomatic episodes, and treatment. As shown in Figure 1, we divided all *KCNJ2* mutation carriers into 2 groups—a typical ATS group (group A): carriers showing 2 or more ATS features, and an atypical ATS group (group B): those showing only 1 of the ATS features or CPVT. Compound mutation and *KCNJ2* double mutation cases were excluded from analysis.

In Vitro Mutagenesis

Regarding four *KCNJ2* mutations found in group B (R82W, R82Q, G144D, and T305S), site-directed mutagenesis was used to construct mutants, as described previously.²³ Briefly, human *KCNJ2* cDNA

was subcloned into the pCMS-EGFP plasmid (Clontech, Palo Alto, CA). We engineered *KCNJ2* mutants using a site-directed mutagenesis kit, QuickChange II XL (Stratagene, La Jolla, CA). The presence of mutations was confirmed by sequencing.

Electrophysiological Experiments and Data Analysis

To assess the functional modulation of *KCNJ2* channels, we used a heterologous expression system with CHO cells.^{8,24} Briefly, the cells were transiently transfected using the Lipofectamine method (Invitrogen, Carlsbad, CA), using a 1.0 $\mu\text{g}/35$ mm dish of pCMSEGFP/*KCNJ2* (wild-type [WT] and/or mutant). For electrophysiological experiments, GFP-positive cells were selected 24 to 72 hours after transfection. Current measurement was conducted using the conventional whole-cell configuration of patch-clamp techniques at 37°C, using an EPC-8 patch-clamp amplifier (HEKA Elektronik; Lambrecht, Germany). Currents were evoked by 150 ms square pulses applied in 10 mV increments to potentials ranging from -140 mV to $+30$ mV from a holding potential of -80 mV. Pipettes were filled with a solution containing (in mmol): K-aspartate, 60; KCl, 65; KH_2PO_4 , 1; MgCl_2 , 2; EDTA, 3; ATP (dipotassium salt), 3; and HEPES, 5 (pH adjusted to 7.2 with KOH), and had a resistance of 3.0 to 5.0 $\text{mol}/\text{L}\Omega$. The bath solution contained (in mmol): NaCl, 140; KCl, 5.4; MgCl_2 , 0.5; CaCl_2 , 1.8; NaH_2PO_4 , 0.33; glucose, 5.5; and HEPES, 5 (pH adjusted to 7.4 with NaOH).²⁵

Immunocytochemistry

The hemagglutinin (HA) epitope (YPYDVPDYA) was introduced into the pCMS-EGFP/*KCNJ2* (WT and mutants) between Ala-115 and Ser-116 (extracellular lesion between TM1 and TM2), as previously described.⁸ CHO cells were transfected with 1.0 μg of plasmid DNA in 35-mm, glass-bottom dishes. Forty-eight hours later, the cells were washed twice with phosphate-buffered saline (PBS), followed by incubation with a mouse anti-HA primary antibody (1:400) (Roche Diagnostics GmbH, Mannheim, Germany) overnight at 4°C. The cells were then washed twice with PBS and incubated with an anti-mouse antibody conjugated to Alexa 568 fluor (1:400) (Molecular Probes, Eugene, OR) as a secondary antibody for 120 minutes, at room temperature. Finally, cells were washed with and immersed in PBS, and confocal images were obtained with a Nikon C1si (Nikon Instruments, Tokyo, Japan).

Statistical Analysis

Clinical data are expressed as the mean \pm SD for continuous variables. Comparisons were performed using the χ^2 test (for counts ≥ 5) and Fisher exact test (for counts < 5) for categorical variables and Wilcoxon test for continuous variables. All analyses of the 45 *KCNJ2* mutation-positive patients and families took into account the relatedness of patients, using a mixed model for continuous data and GEE for categorical data. The electrophysiological current data are shown as mean \pm SEM. A value of $P < 0.05$ was considered significant.

Results

Incidence and Characteristics of *KCNJ2* Mutations in Probands

We identified 16 different *KCNJ2* mutations in 24 of 57 probands (42%) (Table 1 and Figure 1). The mean QUc intervals became longer in ATS with an increasing number of ATS features. Prevalences of *KCNJ2* mutation were 75% (15/20) in typical ATS, 71% (5/7) in mild ATS with a cardiac phenotype alone, 100% (2/2) in mild ATS with periodic paralysis alone, and 7% (2/28) in CPVT.

Table 2 summarizes the genotype/phenotype of *KCNJ2* mutation-positive probands. The mean age at diagnosis of all probands was 18 ± 12 years old. It was significantly younger (14 ± 12 years old) in probands with typical ATS compared

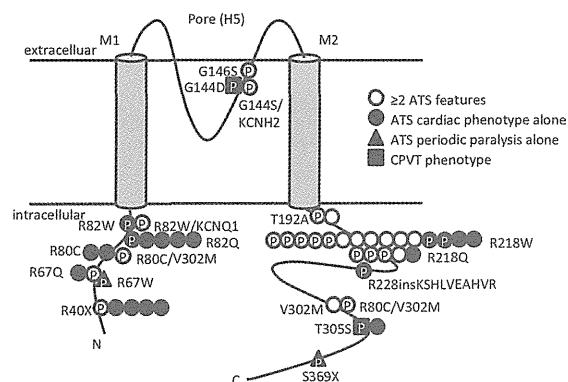


Figure 2. Topology of Kir2.1 channel showing Andersen-Tawil syndrome (ATS)-related mutation sites. **Open circles** indicate probands showing 2 or more ATS features (group A). **Closed symbols** indicate the probands in group B. **Closed circles** indicate those showing ATS with the cardiac phenotype alone; **closed triangles** are ATS with periodic paralysis alone; and **closed squares** represent a clinical diagnosis of CPVT. "P" in each symbol indicates proband.

with those with mild ATS (21 ± 14 years old) or the CPVT phenotype (34 ± 3.5 years old). In 16 *KCNJ2* mutations, 13 (81%) were missense, 2 (13%) nonsense, and 1 (6%) insertion (Table 2 and Figure 2). Six were located in the N terminus, 3 in the pore region, and 9 in the C terminus. Figure 2 depicts the phenotypes and mutation sites of probands and family members. Open circles indicate mutation carriers with 2 or more ATS features (group A), and closed symbols those with atypical ATS (group B); closed circles show the ATS cardiac phenotype alone, closed triangles show periodic paralysis alone, and closed squares show the CPVT phenotype. The letter P in each symbol indicates proband. A 5-year-old boy (case 15, Table 2) was found to have double *KCNJ2* mutations, paternal V302 M, and maternal R80C. Compound mutations were detected in 2 probands: *KCNJ2* R82W plus *KCNH2* P1093L (case 3) and *KCNJ2*-G144S plus *KCNQ1*-A341V (case 4). We excluded these 3 cases from further analyses.

Characteristics of *KCNJ2* Mutation Carriers

After excluding the compound mutation cases, 45 *KCNJ2* mutation carriers (27 females, 21 probands, and 24 of their mutation-positive family members) were enrolled (Table 3). Their mean age at diagnosis was 23 ± 16 years, and the average QUc was 667 ± 50 ms. Regarding arrhythmias, ECGs detected PVC in 30 (67%), bVT in 15 (33%), and pVT in 5 (11%) carriers. One patient had ventricular fibrillation, 4 patients (9%) had syncope, and 11 (24%) received β -blocker therapy.

Prevalence of 3 ATS Features

In 45 *KCNJ2* mutation carriers, ventricular arrhythmias (A) were found in 67% ($n=30$), periodic paralysis (P) in 40% ($n=18$), and dysmorphism (D) in 36% ($n=16$). Abnormal U wave (U) was positive in 88% ($n=38$ of 43) after excluding 2 cases whose U waves were not measured because of the presence of bigeminy. Twenty-one patients (47%) belonged

Table 3. Clinical Characteristics

	Total (n=45)	Group A (n=21)	Group B (n=24)	P Value
Proband, n, (%)	21	12 (57)	9 (38)	0.230
Age at diagnosis, average, y, \pm SD	23 \pm 16	20 \pm 14	26 \pm 16	0.142
Female, n (%)	27 (60)	12 (57)	15 (63)	0.684
Baseline ECG				
HR, average, ms, \pm SD	76 \pm 22	75 \pm 19	77 \pm 25	0.565
QTc, average, ms, \pm SD	430 \pm 42	418 \pm 42	440 \pm 40	0.285
QUc, average, ms, \pm SD	667 \pm 50	695 \pm 52	643 \pm 35	0.004*
T amp, average, mV, \pm SD	0.51 \pm 0.27	0.56 \pm 0.28	0.46 \pm 0.26	0.215
U amp, average, mV, \pm SD	0.21 \pm 0.08	0.24 \pm 0.07	0.18 \pm 0.08	0.024*
Tp-Up, average, ms, \pm SD	214 \pm 31	224 \pm 32	204 \pm 28	0.151
U/T ratio, average, \pm SD	0.57 \pm 0.5	0.66 \pm 0.66	0.48 \pm 0.3	0.601
Arrhythmias, patients, n (%)				
PVC	30 (67)	19 (90)	11 (46)	0.032*
Bidirectional VT	15 (33)	10 (48)	5 (11)	0.195
Polymorphic VT	5 (11)	3 (14)	2 (8)	0.368
VF	1 (2)	0	1 (4)	0.571
Cardiac events				
Syncope, patients, n (%)	4 (9)	2 (10)	2 (8)	0.891
ACA, patients, n (%)	2 (4)	0	2 (8)	0.278
Treatment				
β -blockers	11 (24)	6 (29)	5 (21)	0.589
Flecainide	2 (4)	1 (5)	1 (4)	0.924
Verapamil	2 (4)	1 (5)	1 (4)	0.925
ICD implantation	1 (2)	0	1 (4)	0.533
Mutation site				
C-terminal, patients, n (%)	27 (60)	18 (85)	9 (38)	0.002*
Pore, patients, n (%)	2 (4)	1 (5)	1 (4)	0.925
N-terminal, patients, n (%)	16 (36)	2 (10)	14 (58)	0.001*

ACA indicates aborted cardiac arrest; ICD, implantable cardioverter-defibrillator; VT, ventricular tachycardia; VF, ventricular fibrillation.

Group A: *KCNJ2* mutation carriers showing \geq 2 ATS features; group B: those showing only 1 of the ATS features or catecholaminergic polymorphic ventricular tachycardia; * P <0.05 compared with group A.

to group A (open sections in the pie chart of Figure 3). Six of them (13%) had all 3 features, 7 (16%) both (A) and (P), 7 (16%) both (A) and (D), and 2 (5%) both (D) and (P). On the other hand, 24 patients (53%) with 1 of the ATS features belonged to group B (closed sections of Figure 3): 11 (24%) only (A), 3 (9%) only (P), 2 (4%) only (D). Eight genotype-positive family members (18%) displayed only (U).

CPVT Phenotype in *KCNJ2* Mutation Carriers

We identified 2 *KCNJ2* mutations, G144D (Table 2, case 23) and T305S (case 24), in 2 of 28 probands with CPVT phenotypes (Table 1), without dysmorphic features or periodic paralysis. These 2 cases experienced first syncope after the age of 30 (G144D, 36 years old; T305S, 32 years old). Furthermore, these probands' ECGs showed bidirectional VT at rest as well, and, as in CPVT, exercise-aggravated ventricular arrhythmia. In the G144D case, ECG always showed a PVC bigeminy even at rest, and the exercise stress test increased PVC and produced polymorphic VTs. Flecainide

(150 mg per day) reduced her VTs. In the T305S case, exercise also increased numbers of PVC. She had pVT and VF while nursing her son. Her baseline ECG showed no abnormal U waves (QUc=644 ms, Tpeak-Upeak interval=185 ms).

Comparison of Patients With Typical Versus Atypical Phenotype

Table 3 summarizes the clinical characteristics of patients and compares them between groups A and B. There were no significant differences in the number of probands, age at diagnosis, and sex. Group A had a significantly longer QUc interval (group A, 695 \pm 52 ms versus group B, 643 \pm 35 ms, P =0.004) and higher U wave (0.24 versus 0.18 mV, P =0.024). PVCs were significantly more frequent in group A (n=19 patients versus n=11 patients, P =0.032); however, the incidences of bVT, pVT, and ventricular fibrillation were not different between the 2 groups. There were also no

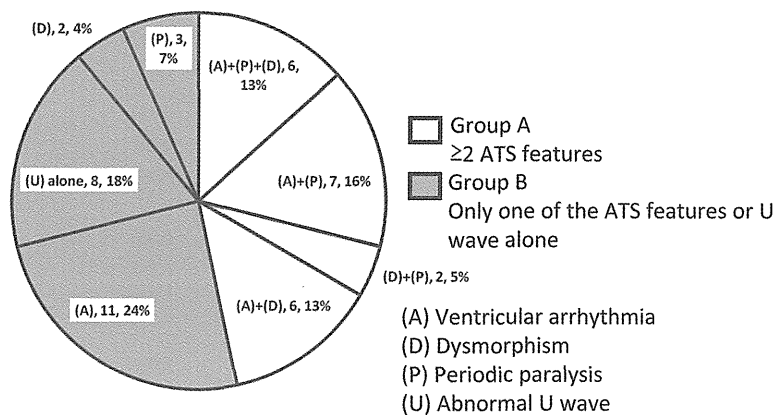


Figure 3. Prevalence of 3 features of Andersen-Tawil syndrome (ATS) among 45 *KCNJ2* mutation carriers (21 probands and 24 family members). (A) indicates ventricular arrhythmia; (P), periodic paralysis; (D), dysmorphic features; (U), abnormal U wave. **Open sections** indicate group A: patients who had ≥ 2 ATS features ($n=21$, 47%). **Closed sections** indicate group B ($n=24$, 53%): those who had only 1 of the ATS features or an abnormal U wave alone.

significant differences regarding the incidence of cardiac events and content of treatment.

Concerning the mutation site, C-terminal mutation carriers were more frequent in group A ($n=18$ versus $n=9$, $P=0.002$). In contrast, N-terminal mutations were more frequent in group B ($n=2$ versus $n=13$, $P=0.001$). As described above, we excluded 1 case with *KCNJ2* double mutations (Table 2, case 15) from this analysis. However his father, carrying a C-terminal mutation alone (V302 M), belonged to group A and showed a full set of ATS features. In contrast, his mother, carrying an N-terminal mutation (R80C), only displayed an abnormal U wave.

Functional Assay of 4 Mutants Found in Atypical Phenotype Group B

We conducted electrophysiological functional assays for 4 mutations in Group B—R82W, R82Q, G144D, and T305S (see Table 2; cases 16, 17, 23, and 24). Figure 4 A-a shows a family of current traces recorded from a CHO cell transfected with WT-*KCNJ2* (1 μg). The lower inset in Figure 4A-a indicates the test pulse protocol. WT-*KCNJ2* expressed ample and time-independent currents showing a strong inward rectification, as depicted in the voltage-current relation in Figure 4B (closed squares). In contrast, all mutants (1 μg) were nonfunctional when expressed alone (Figure 4A-b). To simulate the allelic heterozygosity, WT and each of the mutant-*KCNJ2* clones were cotransfected at an equimolar ratio (0.5 μg each). Representative results are shown in Figure 4A-c. Outward *KCNJ2* channel currents were dominantly suppressed. In contrast, inward currents were variously reduced when coexpressed with WT.

From the results of multiple experiments, the mean current densities were measured at their respective test potentials. In Figure 4B, they are plotted as a function of the potentials, and in Figure 4C, those at -140 and -50 mV are presented as dot plots. Outward current densities at -50 mV when coexpressed with WT-*KCNJ2* were 3.5 ± 1.7 pA/pF in R82Q, 2.3 ± 2.4 pA/pF in R82W, 2.6 ± 0.9 pA/pF in G144D, and 8.1 ± 2.4 pA/pF in T305S. Compared with the current densities obtained with the WT clone alone (1 μg , left plot in Figure 4C), the percent reductions were 95%, 97%, 96%, and 89%, respectively. In contrast, inward current densities at

-140 mV were -162 ± 20 pA/pF in R82Q, -152 ± 22 pA/pF in R82W, -43 ± 13 pA/pF in G144D, and -199 ± 20 pA/pF in T305S. Percent reductions were 58%, 39%, 89%, and 49%, respectively. Thus, G144D mutation exerted dominant negative suppression effects on both outward and inward currents. The other 3 mutations, however, had such effects only on outward currents.

Immunocytochemistry of Mutant Channels (R82Q, R82W, G144D, and T305S)

Regarding several *KCNJ2* mutations, impaired intracellular transport has been reported to cause loss of function. We therefore examined the trafficking of these 4 mutants and WT channels using an HA-tagging method. Figure 5 depicts typical results of confocal imaging. WT and HA-R82Q, HA-R82W, and HA-T305S mutants showed normal trafficking, whereas the HA-G144D mutant displayed no rim of red fluorescence, suggesting the presence of a trafficking defect.

Discussion

Prevalence of *KCNJ2* Mutation and ATS Features in Typical ATS

In the present study, we could identify heterozygous *KCNJ2* mutations in 24 (42%) of 57 probands of different cohorts showing typical ATS, and atypical phenotypes (1 of the ATS features or CPVT). Regarding 20 typical ATS (≥ 2 of 3 ATS features) probands, *KCNJ2* mutations were positive in 15 (75%). This value was comparable to those of previous reports: Plaster et al⁴ identified 13 *KCNJ2* positives in 16 unrelated ATS kindreds (81%). Tristani-Firouzi et al¹² identified 17 *KCNJ2* positives in 25 kindreds (68%), and Donaldson et al²⁶ reported 9 positives in 17 kindreds (53%). The prevalence of *KCNJ2*-positive probands was, however, lower when screened in the total patients, compatible with long-QT syndrome (LQTS): Eckhardt et al²⁷ reported 4 *KCNJ2* mutation positives from 541 LQTS probands (0.74%). Fodstad et al reported 2 carriers in 188 LQTS patients (1%).²⁸

Atypical ATS Phenotype

After excluding the compound mutation cases, there were 45 mutation carriers, and 24 (53%) had atypical ATS phenotypes and 8 had none of them. They only showed abnormal U